First of all we will compare the similarities and differences of MbO_2 and MbCO. They both have the same protein matrix, porphyrin, and central metal atom, a low-spin (0 μ_B) Fe(II). The porphyrin iron binds O_2 under an angle of 115° [15] and exhibits a hydrogen bond to histidine E7.[17] This results in a sterically favored orientation of the oxygen molecule in the porphyrin pocket. In contrast, CO does not show any hydrogen bonding,[18] and its favored linear bonding geometry is not possible due to the histidine E7. The X-ray structure of MbCO shows that the heme "pocket" is widened significantly compared to deoxymyoglobin. For example, the distal histidine moves ca. 140 pm during the binding process.[16] During the dissociation of O_2 from MbO_2, the Fe–O bond and the hydrogen bond to histidine E7 are broken, the heme iron changes its spin from low to high, and the protein "expands" via conformational changes. At the transition state, this process is nearly complete as demonstrated by the large positive volume of activation (+24 cm^3 mol^{-1}).

Contrary to this process, steric tension should first be released during cleavage of the Fe–CO bond. The quantum yield for the photolytical cleavage of the Fe–CO bond is nearly 100%;[5,36] i.e. once the bond has been broken, the ligand nearly always "escapes" into the surroundings. In comparison to O_2, CO must be bound much stronger to the heme iron, since the rate of dissociation of CO is 3 orders of magnitude slower than that of O_2 (see Table IV). This indicates that the Fe–CO bond exhibits stronger σ-donor/π-acceptor characteristics than the Fe–O_2 bond. It follows that Fe–CO bond breakage will be accompanied by a decrease in steric tension and a slight volume collapse due to reorganization of the protein pocket as CO leaves the iron coordination site. If the transition state is relatively "early" during bond *cleavage*, this will result in a volume decrease, i.e. a negative volume of activation (experimental value −4 cm^3 mol^{-1}). By analogy, these arguments support a "late" transition state during Mb–CO bond *formation*. The large negative entropy of activation for the CO off reaction also supports this interpretation. Following this decrease in volume, the completion of bond cleavage is accompanied by the low-to-high spin shift and leads to a volume increase during ligand escape.

As a whole, a total reaction volume of −6 cm^3 mol^{-1} is obtained, inspite of the unfavorable steric situation of bound CO. For both O_2 and CO the outlined effects lead to an overall negative reaction volume; the difference in the reaction volumes ($\Delta\bar{V}(O_2) - \Delta\bar{V}(CO)$) is −13 cm^3 mol^{-1}. The arguments in the above section lead to the conclusion that the mechanism of ligand binding must be the determining factor to account for this difference, which in total means a larger volume decrease for O_2. The reasons for this may be the different bonding characters for O_2 and CO, the bonding angles, hydrogen bonding effects, and conformational changes resulting from these factors. In terms of bonding character it may also be appropriate to think of the bonding modes as Fe^{III}–O_2^- and Fe^{II}–CO, respectively, which would further account for the significantly different volume profiles reported in this paper.

In summary, the reactions of oxygen and carbon monoxide proceed according to two different mechanisms. Whereas the entry of the ligand into the protein is the rate-determining step for the binding of oxygen, bond formation is the crucial factor for carbon monoxide. Hence, entry and "migration" through the protein is rate-determining for O_2, as indicated by the rate constant of the bond formation reaction, but for CO these processes are only of minor importance. Bond cleavage, however, is the rate-determining step during the dissociation reaction for both ligands, and here the transition state for oxygen strongly resembles the product state, i.e. Mb + O_2. CO is however still tightly bound in the transition state. The negative volume of activation for Mb–CO bond *cleavage* corresponds to the positive volume of activation for bond *formation* between Mb and O_2, in that the sign of the activation volumes for both reactions is contrary to that generally expected. As outlined above, the reason for these effects is related to the bonding mechanism of both ligands, which at different locations of the reaction coordinate can result in different contributions from conformational changes.

Acknowledgment. We gratefully acknowledge financial support from the Deutsche Forschungsgemeinschaft and the Fonds der Chemischen Industrie.

Registry No. CO, 630-08-0; O_2, 7782-44-7.

Contribution from the Department of Chemistry and Laboratory for Molecular Structure and Bonding, Texas A&M University, College Station, Texas 77843

New Di- and Trinuclear Complexes of Ruthenium with Octahedra Joined on Faces or Edges. 3.[1] New Trinuclear Compounds of the Type $[(R_3P)_2ClRuCl_3RuCl_3RuCl(PR_3)_2]^n$ (n = 0, +1): Structures, EPR Spectroscopy, Electrochemistry, and Molecular Orbitals

F. Albert Cotton* and Raymund C. Torralba

Received December 14, 1990

We report here the preparation and characterization of four new compounds of the type $(R_3P)_2ClRuCl_3RuCl_3RuCl(PR_3)_2$ as well as a cationic oxidation product of one of them. The new compounds that have been crystallographically characterized are as follows: $Ru_3Cl_8(PEt_3)_4$ (**3**), monoclinic, space group $P2_1/n$, a = 11.041 (5) Å, b = 14.484 (5) Å, c = 12.939 (4) Å, β = 102.92 (3)°, V = 2106 (3) Å^3, Z = 2, Ru–Ru = 2.862 (1) Å; $Ru_3Cl_8(PMe_3)_4$ (**4a**), monoclinic, space group $P2_1/n$, a = 13.292 (3) Å, b = 7.128 (1) Å, c = 16.667 (5) Å, β = 109.16 (2)°, V = 1491.6 (6) Å^3, Z = 2, Ru–Ru = 2.828 (1) Å; $Ru_3Cl_8(PMe_3)_4 \cdot C_6H_6$ (**4b**), triclinic, space group $P\bar{1}$, a = 9.038 (4) Å, b = 13.253 (4) Å, c = 7.503 (2) Å, α = 101.31 (2)°, β = 100.00 (3)°, γ = 97.09 (3)°, V = 856.2 (5) Å^3, Z = 1, Ru–Ru = 2.842 (0) Å; $[Ru_3Cl_8(PEt_3)_4][SbF_6]$ (**5**), monoclinic, space group $P2_1/a$, a = 14.558 (5) Å, b = 31.81 (2) Å, c = 15.049 (6) Å, β = 93.95 (3)°, V = 6952 (9) Å^3, Z = 6, average Ru–Ru = 2.906 (3) Å. In addition, $Ru_3Cl_8(PMe_2Ph)_4$ (**2**) and the PMe_3 (**6**) and PBu_3 (**7**) homologues of **5** are reported. Together with the previously reported $Ru_3Cl_8(PBu_3)_4$ (**1**), this gives four such molecules, one (with PMe_3) known in two crystal forms. A detailed SCF–Xα–SW study of these species is reported and compared with previous results for $[Ru_3Cl_{12}]^{4-}$. The electrochemistry of all four of these molecules and of **5** as well as the EPR spectrum of **5** are presented and discussed. From the electrochemistry as well as by reactions with $AgSbF_6$, Cp_2Co, and Na/Hg, it has been shown that besides the neutral molecules the +1, −1, and −2 ions also exist, although only the first has so far been isolated and characterized as compound **5**.

Introduction

In 1980, the first trinuclear complex consisting of three octahedra sharing faces in a linear array was reported.[2] This was the $[Ru_3Cl_{12}]^{4-}$ ion, and its electronic structure was later investigated in detail by means of SCF–Xα–SW calculations.[3] The

0020-1669/91/1330-3293$02.50/0

Table I. Crystal Data for Compounds **3** and **5**

	3	**5**
formula	$Ru_3Cl_8P_4C_{24}H_{60}$	$SbRu_3Cl_8P_4F_6C_{24}BH_{60}$
fw	1059.5	1295.22
space group	$P2_1/n$	$P2_1/a$
syst abs	$h0l$, $h + l = 2n + 1$ $0k0$, $k = 2n + 1$	$h0l$, $h = 2n + 1$ $0k0$, $k = 2n + 1$
a, Å	11.041 (5)	14.558 (5)
b, Å	14.484 (5)	31.81 (2)
c, Å	12.939 (4)	15.049 (3)
α, deg	90	90
β, deg	102.92 (3)	93.95 (3)
γ, deg	90	90
V, Å	2106 (3)	6952 (9)
Z	2	6
d_{calc}, g/cm	1.744	1.178
cryst size, mm	0.15 × 0.08 × 0.10	0.22 × 0.12 × 0.30
μ(Mo Kα), cm^{-1}	17.986	14.450
data collcn instrum	Rigaku AFC5R	Rigaku AFC5R
radiation (monochromated in incident beam)	Mo Kα (λ_α = 0.71073 Å)	Mo Kα (λ_α = 0.71073 Å)
orientation reflcns: no.; range (2θ), deg	21; $10 < 2\theta < 21$	24; $18 < 2\theta < 27$
temp, °C	21 ± 1	21 ± 1
scan method	2θ–ω	ω
data collcn range (2θ), deg	$4 < 2\theta < 50$	$4 < 2\theta < 50$
no. of unique data; tot. no. with $F_o > 3\sigma(F_o)$	2794; 1880	12225; 3831
no. of params refined	179	614
transm factors, %: max; min	0.999; 0.914	1.00; 0.775
R^a	0.0579	0.0663
R_w^b	0.0845	0.0820
quality-of-fit indicator^c	1.521	1.462
largest shift/esd, final cycle	0.00	0.358
largest peak, e/Å^3	0.949	0.749

$^a R = \sum||F_o| - |F_c||/\sum|F_o|$. $^b R_w = [\sum w(|F_o| - |F_c|)/\sum w|F_o|]^{1/2}$; $w = 1/\sigma(|F_o|)$. ^{c}Quality-of-fit = $[\sum w(|F_o| - |F_c|)/(N_{observns} - N_{params})]^{1/2}$.

Table II. Crystal data for Compounds **4a** and **4b**

	4a	**4b**
formula	$Ru_3Cl_8P_4C_{12}H_{36}$	$Ru_3Cl_8P_4C_{18}BH_{42}$
fw	891.15	969.25
space group	$P2_1/n$	$P\bar{1}$
syst abs	$h0l$, $h + l = 2n + 1$ $0k0$, $k = 2n + 1$	none
a, Å	13.292 (3)	9.038 (4)
b, Å	7.128 (1)	13.253 (2)
c, Å	16.667 (5)	7.503 (2)
α, deg	90	101.31 (2)
β, deg	109.16 (2)	100.00 (3)
γ, deg	90	97.09 (3)
V, Å	1491.6 (6)	856.2 (5)
Z	2	1
d_{calc}, g/cm	1.984	1.880
cryst size, mm	0.30 × 0.08 × 0.15	0.40 × 0.12 × 0.35
μ(Mo Kα), cm^{-1}	24.129	21.096
data collcn instrum	Rigaku AFC5R	Rigaku AFC5R
radiation (monochromated in incident beam)	Mo Kα (λ_α = 0.71073 Å)	Mo Kα (λ_α = 0.71073 Å)
orientation reflcns no.; range (2θ), deg	25; $18 < 2\theta < 25$	24; $18 < 2\theta < 27$
temp, °C	21 ± 1	21 ● 1
scan method	2θ–ω	2θ–ω
data collcn range (2θ), deg	$4 < 2\theta < 50$	$3 < 2\theta < 50$
no. of unique data; tot. no. with $F_o > 3\sigma(F_o)$	2634; 1748	3686; 3302
no. of params refined	124	216
transm factors, %: max; min	1.00; 0.876	1.00; 0.77
R^a	0.0417	0.0260
R_w^b	0.0614	0.0350
quality-of-fit indicator^c	1.362	0.914
largest shift/esd, final cycle	0.00	0.19
largest peak, e/Å^3	1.608	0.887

$^a R = \sum||F_o| - |F_c||/\sum|F_o|$. $^b R_w = [\sum w(|F_o| - |F_c|)/\sum w|F_o|]^{1/2}$; $w = 1/\sigma(|F_o|)$. ^{c}Quality-of-fit = $[\sum w(|F_o| - |F_c|)/(N_{observns} - N_{params})]^{1/2}$.

$Ru_3Cl_8(PH_3)_4$ $16b_u$ orbital

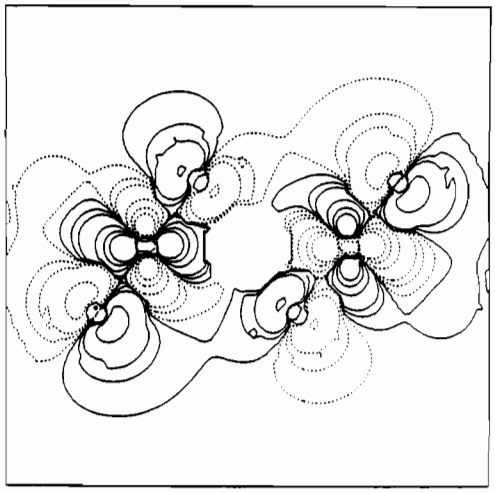

Figure 1. Contour plot of the $16b_u$ MO of $Ru_3Cl_8(PH_3)_4$, the HOMO. (by SCF-Xα-SW).

$Ru_3Cl_8(PH_3)_4$ $11a_u$ orbital

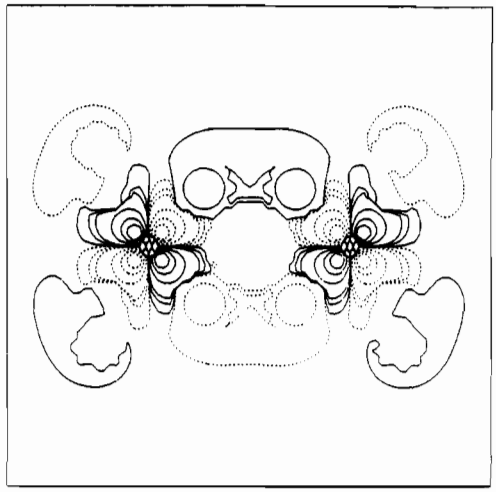

Figure 2. Contour plot of the $11a_u$ MO of $Ru_3Cl_8(PH_3)_4$. (by SCF-Xα-SW).

stability of this complex, in which the formation of delocalized Ru–Ru bonding leads to a closed-shell ground state, encouraged the hope that related compounds would also exist. In 1989, we were able to report[4] that this hope had been fulfilled by the preparation and structural characterization of the molecular species $(PBu_3)_2ClRuCl_3RuCl_3RuCl(PBu_3)_2$ (**1**). We now wish to describe work that considerably extends that chemistry and enhances our understanding of the electronic structures of the $L_2ClRuCl_3RuCl_3RuClL_2$ species in general.

(1) Part 2: Cotton, F. A.; Torralba, R. C. *Inorg. Chem.* **1991**, *30*, 2196.
(2) Bino, A.; Cotton, F. A. *J. Am. Chem. Soc.* **1980**, *102*, 608.
(3) Bursten, B. E.; Cotton, F. A.; Fang, A. *Inorg. Chem.* **1983**, *22*, 2127.
(4) Cotton, F. A.; Matusz, M.; Torralba, R. C. *Inorg. Chem.* **1989**, *28*, 1516.

Table III. Positional and Isotropic Equivalent Thermal Displacement Parameters (B_{iso} in Å^2) for $Ru_3Cl_8(PEt_3)_4$ (**3**)[a]

atom	x	y	z	B_{iso}
Ru(1)	0.0766 (1)	0.34278 (8)	0.1325 (1)	1.88 (3)
Ru(2)	0.000	0.500	0.000	2.08 (4)
Cl(1)	−0.1323 (4)	0.3738 (3)	0.0154 (3)	2.9 (1)
Cl(2)	0.1510 (4)	0.3917 (3)	−0.0258 (3)	3.1 (1)
Cl(3)	0.0776 (4)	0.4994 (3)	0.1851 (3)	2.68 (9)
Cl(4)	0.0749 (4)	0.1893 (3)	0.0762 (3)	3.2 (1)
P(1)	0.2797 (4)	0.3346 (3)	0.2315 (3)	2.23 (9)
P(2)	−0.0163 (4)	0.2899 (3)	0.2661 (4)	2.4 (1)
C(11)	0.307 (2)	0.358 (1)	0.373 (1)	3.2 (4)
C(12)	0.309 (2)	0.458 (1)	0.410 (1)	4.2 (5)
C(13)	0.356 (2)	0.221 (1)	0.231 (1)	2.7 (4)
C(14)	0.394 (2)	0.197 (1)	0.128 (2)	4.0 (5)
C(15)	0.385 (1)	0.418 (1)	0.187 (1)	3.4 (5)
C(16)	0.522 (2)	0.415 (1)	0.249 (2)	5.2 (6)
C(21)	0.057 (2)	0.183 (1)	0.330 (1)	3.6 (5)
C(22)	0.010 (2)	0.146 (1)	0.422 (2)	5.7 (7)
C(23)	−0.017 (2)	0.371 (1)	0.377 (1)	3.9 (5)
C(24)	−0.118 (2)	0.446 (1)	0.356 (2)	5.8 (7)
C(25)	−0.179 (2)	0.261 (1)	0.225 (2)	4.4 (5)
C(26)	−0.216 (2)	0.180 (2)	0.162 (2)	8.0 (9)
H(1)	0.396 (2)	0.329 (1)	0.409 (1)	6.0 (9)*
H(2)	0.235 (2)	0.324 (1)	0.402 (1)	6.0 (9)*
H(3)	0.326 (2)	0.460 (1)	0.495 (1)	6.0 (9)*
H(4)	0.220 (2)	0.490 (1)	0.376 (1)	6.0 (9)*
H(5)	0.382 (2)	0.495 (1)	0.384 (1)	6.0 (9)*
H(6)	0.293 (2)	0.169 (1)	0.246 (1)	6.0 (9)*
H(7)	0.439 (2)	0.221 (1)	0.294 (1)	6.0 (9)*
H(8)	0.437 (2)	0.130 (1)	0.136 (2)	6.0 (9)*
H(9)	0.458 (2)	0.249 (1)	0.112 (2)	6.0 (9)*
H(10)	0.312 (2)	0.196 (1)	0.064 (2)	6.0 (9)*
H(11)	0.349 (1)	0.487 (1)	0.193 (1)	6.0 (9)*
H(12)	0.383 (1)	0.403 (1)	0.104 (1)	6.0 (9)*
H(13)	0.575 (2)	0.466 (1)	0.216 (2)	6.0 (9)*
H(14)	0.560 (2)	0.348 (1)	0.242 (2)	6.0 (9)*
H(15)	0.526 (2)	0.431 (1)	0.331 (2)	6.0 (9)*
H(16)	0.155 (2)	0.197 (1)	0.357 (1)	6.0 (9)*
H(17)	0.044 (2)	0.130 (1)	0.270 (1)	6.0 (9)*
H(18)	0.061 (2)	0.084 (1)	0.451 (2)	6.0 (9)*
H(19)	−0.088 (2)	0.130 (1)	0.396 (2)	6.0 (9)*
H(20)	0.024 (2)	0.197 (1)	0.484 (2)	6.0 (9)*
H(21)	0.072 (2)	0.405 (1)	0.397 (1)	6.0 (9)*
H(22)	−0.030 (2)	0.330 (1)	0.444 (1)	6.0 (9)*
H(23)	−0.109 (2)	0.488 (1)	0.426 (2)	6.0 (9)*
H(24)	−0.208 (2)	0.414 (1)	0.338 (2)	6.0 (9)*
H(25)	−0.106 (2)	0.488 (1)	0.290 (2)	6.0 (9)*
H(26)	−0.224 (2)	0.319 (1)	0.181 (2)	6.0 (9)*
H(27)	−0.212 (2)	0.252 (1)	0.297 (2)	6.0 (9)*
H(28)	−0.316 (2)	0.174 (2)	0.145 (2)	6.0 (9)*
H(29)	−0.175 (2)	0.120 (2)	0.204 (2)	6.0 (9)*
H(30)	−0.187 (2)	−0.187 (2)	0.088 (2)	6.0 (9)*

[a] Values of B for anisotropically refined atoms are given in the form of the equivalent isotropic displacement parameter defined as $(4/3)[a^2B_{11} + b^2B_{22} + c^2B_{33} + ab(\cos\gamma)B_{12} + ac(\cos\beta)B_{13} + bc(\cos\alpha)B_{23}]$. Starred values denote atoms that were refined isotropically. The numbers in parentheses are the estimated standard deviations in the least significant digit.

Table IV. Positional and Isotropic Equivalent Thermal Displacement Parameters (B_{iso} in Å^2) for $Ru_3Cl_8(PMe_3)_4$ (**4a**)[a]

atom	x	y	z	B_{iso}
Ru(1)	0.000	0.000	0.000	2.45 (2)
Ru(2)	−0.20823 (5)	−0.0757 (1)	0.00150 (4)	2.50 (1)
Cl(1)	−0.1525 (2)	0.1747 (4)	−0.0755 (2)	3.37 (5)
Cl(2)	−0.0514 (2)	0.0321 (4)	0.1230 (1)	3.30 (5)
Cl(3)	0.0911 (2)	0.2880 (3)	0.0333 (2)	3.31 (5)
Cl(4)	−0.3315 (2)	0.1219 (4)	0.0331 (2)	4.08 (5)
P(1)	−0.2424 (2)	−0.2842 (4)	0.0951 (2)	3.17 (5)
P(2)	−0.3347 (2)	−0.1761 (4)	−0.1218 (2)	3.58 (6)
C(1)	−0.1565 (8)	−0.491 (1)	0.1197 (7)	4.2 (3)
C(2)	−0.3794 (8)	−0.380 (2)	0.0701 (7)	4.8 (3)
C(3)	−0.2237 (8)	−0.177 (2)	0.2002 (6)	4.6 (3)
C(4)	−0.348 (1)	−0.432 (2)	−0.1372 (8)	6.2 (4)
C(5)	−0.4682 (8)	−0.097 (2)	−0.1386 (8)	6.6 (4)
C(6)	−0.309 (1)	−0.103 (2)	−0.2190 (6)	6.2 (3)

[a] Values of B for anisotropically refined atoms are given in the form of the equivalent isotropic displacement parameter defined as $(4/3)[a^2B_{11} + b^2B_{22} + c^2B_{33} + ab(\cos\gamma)B_{12} + ac(\cos\beta)B_{13} + bc(\cos\alpha)B_{23}]$. The numbers in parentheses are the estimated standard deviations in the least significant digit.

Table V. Positional and Isotropic Equivalent Thermal Displacement Parameters (B_{iso} in Å^2) for $Ru_3Cl_8(PMe_3)_4 \cdot C_6H_6$ (**4b**)[a]

atom	x	y	z	B_{iso}
Ru(1)	0.000	0.500	0.000	2.165 (5)
Ru(2)	0.09116 (2)	0.31013 (1)	0.06309 (2)	2.055 (3)
Cl(1)	0.10594 (8)	0.46645 (5)	0.28845 (8)	2.85 (1)
Cl(2)	−0.16365 (7)	0.33685 (5)	−0.08755 (9)	2.82 (1)
Cl(3)	0.18325 (7)	0.41926 (5)	−0.14172 (8)	2.96 (1)
Cl(4)	0.08517 (8)	0.15502 (5)	−0.1541 (1)	3.58 (1)
P(1)	0.33673 (8)	0.30352 (6)	0.2054 (1)	3.13 (1)
P(2)	−0.03639 (7)	0.21149 (5)	0.22778 (8)	2.38 (1)
C(1)	0.6136 (4)	0.9624 (3)	0.4231 (5)	6.24 (8)
C(2)	0.4678 (6)	0.9091 (3)	0.3689 (5)	6.3 (1)
C(3)	0.6446 (4)	1.0532 (3)	0.5553 (5)	5.89 (9)
C(11)	0.4013 (4)	0.1780 (3)	0.1631 (5)	4.85 (8)
C(12)	0.3837 (4)	0.3442 (3)	0.4573 (5)	5.17 (8)
C(13)	0.4803 (4)	0.3886 (3)	0.1413 (6)	6.6 (1)
C(21)	−0.1997 (3)	0.1219 (2)	0.0840 (4)	3.81 (6)
C(22)	0.0618 (4)	0.1241 (2)	0.3451 (5)	4.39 (7)
C(23)	−0.1141 (4)	0.2863 (3)	0.4068 (4)	4.30 (7)
H(1)	0.414 (5)	0.170 (3)	0.041 (6)	3.9 (2)*
H(2)	0.333 (5)	0.128 (3)	0.205 (6)	3.9*
H(3)	0.501 (5)	0.192 (3)	0.240 (6)	3.9*
H(4)	0.323 (5)	0.304 (3)	0.510 (6)	3.9*
H(5)	0.369 (5)	0.421 (3)	0.508 (5)	3.9*
H(6)	0.490 (4)	0.349 (3)	0.515 (5)	3.9*
H(7)	0.586 (5)	0.382 (3)	0.201 (6)	3.9*
H(8)	0.453 (5)	0.452 (3)	0.171 (6)	3.9*
H(9)	0.473 (4)	0.362 (3)	0.008 (5)	3.9*
H(10)	−0.246 (4)	0.082 (3)	0.143 (5)	3.9*
H(11)	−0.277 (5)	0.161 (3)	0.036 (6)	3.9*
H(12)	−0.170 (5)	0.085 (3)	0.004 (6)	3.9*
H(13)	−0.009 (5)	0.090 (3)	0.388 (6)	3.9*
H(14)	0.137 (5)	0.159 (3)	0.430 (6)	3.9*
H(15)	0.097 (5)	0.090 (3)	0.250 (6)	3.9*
H(16)	−0.165 (5)	0.334 (3)	0.357 (6)	3.9*
H(17)	−0.033 (4)	0.321 (3)	0.500 (5)	3.9*
H(18)	−0.178 (5)	0.237 (3)	0.449 (5)	3.9*
H(19)	0.672 (5)	0.938 (3)	0.360 (6)	5.0 (6)*
H(20)	0.448 (5)	0.847 (3)	0.288 (6)	5.0*
H(21)	0.748 (5)	1.085 (3)	0.589 (6)	5.0*

[a] B values for anisotropically refined atoms are given in the form of the equivalent isotropic displacement parameter defined as $(4/3)[a^2B_{11} + b^2B_{22} + c^2B_{33} + ab(\cos\gamma)B_{12} + ac(\cos\beta)B_{13} + bc(\cos\alpha)B_{23}]$. Starred values denote atoms that were refined isotropically. The numbers in parentheses are the estimated standard deviations in the least significant digit.

Experimental Section

All chemical reactions and operations, unless otherwise indicated, were done under an argon atmosphere by employing standard vacuum-line techniques.[5] All solvents were predried over 8–12 mesh molecular sieves and freshly distilled under nitrogen prior to use. CH_2Cl_2 was distilled over P_2O_5; benzene, n-hexane, toluene, and tetrahydrofuran (THF) were distilled from Na–K/benzophenone; methanol was distilled from Mg. $RuCl_3 \cdot 3H_2O$ was purchased from Aldrich Chemical Co. and was either used as received or heated under vacuum for 1 h before mixing it with other chemicals. PBu_3, PEt_3, PMe_3, and PMe_2Ph (Strem Chemicals) were transferred into Schlenk tubes and kept under argon. These were stored in the refrigerator when not in use. $AgSbF_6$ and $(\eta^5\text{-}C_5H_5)_2Co^{II}$ (Aldrich) were kept under nitrogen in the drybox. $(C_4H_9)_4NPF_6$ (Aldrich) was recrystallized before use. Na/Hg amalgam was prepared by dissolving bits of Na metal in Hg that was pumped on for at least 1 h. Triple distilled grade Hg (D. F. Goldsmith Chemical and Metal Corp.) and Na metal (J. T. Baker Chemical Co.) were used as received. Ph_4AsCl, Ph_4PCl, [PPN]Cl, ($PPN^+ = Ph_3PNPPh_3^+$), and 15-crown-5

(5) Shriver, D. F.; Drezden, M. A. *The Manipulation of Air-Sensitive Compounds*, 2nd Ed.; Wiley: New York, 1986.

Table VI. Positional and Isotropic Equivalent Thermal Displacement Parameters (B_{iso} in Å^2) for $[Ru_3Cl_8(PEt_3)_4][SbF_6]$ (**5**)[a]

atom	x	y	z	B_{iso}
Sb(1)	−0.500	0.500	0.000	5.82 (8)
Sb(2)	−0.4264 (2)	0.35545 (9)	−0.5191 (2)	9.08 (9)
Ru(1)	−0.6215 (1)	0.18082 (7)	−0.1115 (1)	4.53 (6)
Ru(2)	−0.4887 (1)	0.17004 (6)	0.0307 (1)	4.63 (6)
Ru(3)	−0.3314 (1)	0.16108 (6)	0.1714 (1)	3.86 (5)
Ru(4)	−0.500	0.000	−0.500	4.54 (8)
Ru(5)	−0.3631 (1)	0.01798 (6)	−0.3566 (1)	3.97 (5)
Cl(1)	−0.7610 (5)	0.2147 (3)	−0.1144 (5)	7.1 (2)
Cl(2)	−0.4788 (4)	0.1468 (2)	−0.1160 (4)	5.2 (2)
Cl(3)	−0.6401 (4)	0.1461 (2)	0.0344 (4)	5.2 (2)
Cl(4)	−0.5457 (4)	0.2358 (2)	−0.0152 (4)	5.6 (2)
Cl(5)	−0.3369 (4)	0.1961 (2)	0.0315 (4)	4.4 (2)
Cl(6)	−0.4898 (4)	0.1913 (2)	0.1807 (4)	4.7 (2)
Cl(7)	−0.4261 (4)	0.1059 (2)	0.0870 (4)	4.9 (2)
Cl(8)	−0.3323 (4)	0.1232 (2)	0.2999 (4)	6.0 (2)
Cl(9)	−0.4724 (4)	0.0023 (2)	0.3469 (4)	5.0 (2)
Cl(10)	−0.3568 (4)	−0.0325 (2)	−0.4699 (4)	4.5 (2)
Cl(11)	−0.4295 (4)	0.0658 (2)	−0.4764 (4)	5.2 (2)
Cl(12)	−0.3711 (5)	0.0691 (2)	−0.2495 (4)	6.3 (2)
P(1)	−0.6912 (5)	0.1203 (3)	−0.1794 (S)	6.6 (2)
P(2)	−0.5896 (6)	0.2220 (3)	−0.2353 (6)	8.8 (3)
P(3)	−0.6911 (4)	0.3683 (2)	0.1374 (5)	4.6 (2)
P(4)	−0.2691 (4)	0.2190 (2)	0.2510 (5)	4.6 (2)
P(5)	−0.2137 (5)	0.0416 (2)	−0.3792 (5)	5.6 (2)
P(6)	−0.6784 (4)	0.0351 (2)	0.2517 (5)	4.9 (2)
F(1)	−0.544 (1)	0.4535 (7)	−0.062 (1)	12.8 (8)
F(2)	−0.474 (2)	0.4653 (7)	0.090 (2)	14.9 (9)
F(3)	−0.385 (1)	0.4921 (6)	−0.041 (2)	12.8 (8)
F(4)	−0.549 (2)	0.347 (1)	−0.510 (3)	25 (2)
F(5)	−0.443 (2)	0.3356 (9)	−0.638 (2)	16 (1)
F(6)	−0.417 (2)	0.373 (1)	−0.408 (2)	24 (2)
F(7)	−0.393 (4)	0.309 (1)	−0.490 (3)	49 (3)
F(8)	−0.319 (2)	0.375 (2)	−0.542 (3)	30 (2)
F(9)	−0.466 (3)	0.404 (1)	−0.564 (3)	26 (2)
C(1)	−0.635 (2)	0.0716 (8)	−0.135 (3)	11 (1)
C(2)	−0.685 (2)	0.031 (1)	−0.161 (3)	11 (1)
C(3)	−0.821 (3)	0.118 (1)	−0.169 (3)	11 (1)
C(4)	−0.846 (3)	0.112 (1)	−0.081 (3)	15 (2)
C(5)	−0.704 (4)	0.118 (1)	−0.292 (4)	17 (2)
C(6)	−0.633 (6)	0.106 (2)	−0.337 (4)	34 (4)
C(7)	−0.682 (3)	0.222 (1)	−0.326 (2)	13 (2)
C(8)	−0.680 (4)	0.250 (2)	−0.399 (3)	19 (3)
C(9)	−0.565 (4)	0.277 (2)	−0.218 (3)	18 (2)
C(10)	−0.630 (5)	0.300 (2)	−0.178 (4)	21 (3)
C(11)	−0.462 (4)	0.228 (2)	−0.266 (4)	22*
C(12)	−0.460 (5)	0.197 (2)	−0.334 (6)	39*
C(13)	−0.702 (2)	0.4105 (9)	0.056 (2)	5.9 (8)
C(14)	−0.729 (2)	0.396 (1)	−0.043 (2)	9 (1)
C(15)	−0.613 (1)	0.3293 (8)	0.091 (2)	5.9 (8)
C(16)	−0.525 (2)	0.3499 (9)	0.055 (2)	8 (1)
C(17)	−0.623 (2)	0.3940 (9)	0.236 (2)	7.1 (9)
C(18)	−0.647 (3)	0.441 (1)	0.246 (2)	12 (1)
C(19)	−0.159 (2)	0.209 (1)	0.319 (2)	7.2 (9)
C(20)	−0.124 (2)	0.2481 (9)	0.370 (2)	8 (1)
C(21)	−0.241 (2)	0.2657 (8)	0.179 (2)	6.2 (8)
C(22)	−0.330 (2)	0.2886 (8)	0.143 (2)	6.3 (8)
C(23)	−0.345 (2)	0.2425 (9)	0.332 (2)	6.7 (9)
C(24)	−0.367 (2)	0.213 (1)	0.411 (2)	8 (1)
C(25)	−0.143 (2)	0.003 (1)	−0.444 (2)	10 (1)
C(26)	−0.156 (3)	0.009 (1)	−0.542 (3)	15 (2)
C(27)	−0.142 (2)	0.0509 (9)	−0.271 (2)	7.3 (9)
C(28)	−0.043 (2)	0.064 (1)	−0.287 (2)	10 (1)
C(29)	−0.208 (2)	0.090 (1)	−0.442 (2)	9 (1)
C(30)	−0.245 (3)	0.130 (1)	−0.396 (3)	11 (1)
C(31)	−0.595 (2)	0.0802 (8)	0.249 (2)	6.3 (8)
C(32)	−0.593 (2)	0.1084 (8)	0.333 (2)	8 (1)
C(33)	−0.787 (2)	0.0618 (8)	0.272 (2)	6.2 (8)
C(34)	−0.816 (2)	0.096 (1)	0.201 (2)	9 (1)
C(35)	−0.693 (2)	0.0164 (9)	0.137 (2)	7.3 (9)
C(36)	−0.598 (2)	0.009 (1)	0.097 (2)	12 (1)

[a] B values for anisotropically refined atoms are given in the form of the equivalent isotropic displacement parameter defined as $(4/3)[a^2B_{11} + b^2B_{22} + c^2B_{33} + ab(\cos\gamma)B_{12} + ac(\cos\beta)B_{13} + bc(\cos\alpha)B_{23}]$. The numbers in parentheses are the estimated standard deviations in the least significant digit. Starred values denote atoms that have fixed thermal parameters.

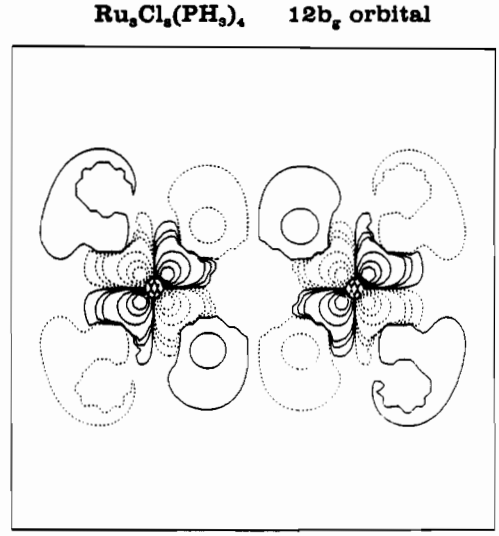

Figure 3. Contour plot of the $12b_g$ MO of $Ru_3Cl_8(PH_3)_4$. (by SCF–Xα–SW).

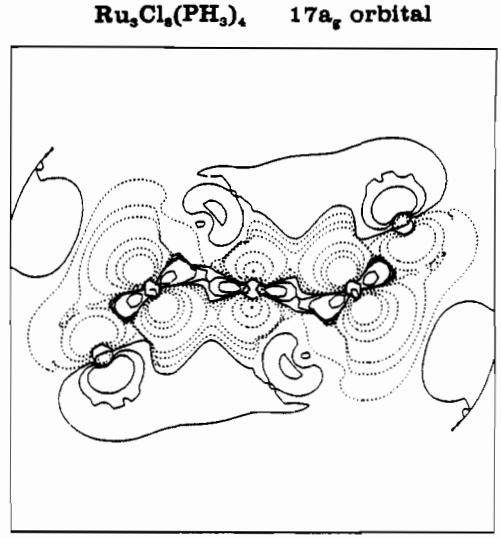

Figure 4. Contour plot of the $17a_g$ MO of $Ru_3Cl_8(PH_3)_4$. (by SCF–Xα–SW).

(Aldrich) were used as received. The 15-crown-5 was refrigerated and kept under argon when not being used.

The electronic absorption spectra in CH_2Cl_2 were recorded on a Cary 17D spectrophotometer. Cyclic voltammetric studies were carried out by using a BAS 100 electrochemical analyzer. All CV studies were done in CH_2Cl_2 solutions with $(C_4H_9)_4NPF_6$ as supporting electrolyte and Ag/AgCl as reference electrode. The scan rate used for all reported results was 100 mV/s unless indicated otherwise. Under these conditions Cp_2Fe had $E_{1/2}$ at 0.42–0.47 V.

Magnetic susceptibilities of the solid bulk samples for compounds **1** and **3** were obtained by the Guoy method using a Johnson Matthey magnetic balance. For CH_2Cl_2 solutions of compounds **5**, **8**, and **9**, the Evans method[6] was used, employing the EM390 NMR spectrometer at 90 MHz. ESR spectra of frozen CH_2Cl_2–toluene solutions of compounds **5** and **9** were recorded at 77 K by an IBM Instruments, Inc., ER200D-SRC spectrometer equipped with a Bruker ER082(155/45) magnet. ^{31}P NMR spectra were recorded on a XL200 Varian spectrometer at 81 MHz. Chemical shifts were referenced to external 85% H_3PO_4.

Preparation of $Ru_3Cl_8(PMe_2Ph)_4$ (2). A 0.57-g (2.2-mmol) sample of $RuCl_3 \cdot 3H_2O$ was dissolved in 5 mL of methanol, and 0.41 g (2.9 mmol) of PMe_2Ph was added. A dark colored precipitate immediately formed. The solid material, 0.52 g, was isolated by filtration after 2 h more of stirring. A 0.1-g sample of the crude product was recrystallized by layering its CH_2Cl_2 solution with 2–3 times its volume of methanol

(6) Evans, D. F. *J. Chem. Soc.* **1959**, 2003.

Table VII. Upper Valence MOs for $Ru_3Cl_8(PH_3)_4$ from SCF-Xα-SW Calculations

levels[a]	energy, eV	% contribn[b]									Ru_1 angular contribn[c]		
		Ru_1	Ru_2	Cl_1	Cl_2	Cl_3	P	H	int	out	s	p	d
$14b_g$	−4.539	50	1	0	10	0	25	2	12	0	4	96	
$12a_u$	−4.544	51	0	0	9	0	25	3	12	0		5	95
$20a_g$	−4.978	54	2	9	3	12	9	1	9	0	1	1	98
$17b_u$	−5.037	1	58	0	33	0	1	0	7	0	1	1	98
$13b_g$	−6.160	1	58	0	33	0	1	0	7	0			
$19a_g$	−6.267	3	58	20	11	1	1	0	7	0			
$18a_g$	−7.788	58	28	2	3	3	0	1	4	0			100
$16b_u$ (HOMO)	−8.295	78	0	3	3	8	0	1	7	0			100
$11a_u$	−8.341	79	0	2	1	9	0	1	7	0			100
$12b_g$	−8.344	78	1	3	1	9	0	1	7	0			100
$17a_g$	−8.499	76	6	0	7	1	1	2	3	0			99
$15b_u$	−8.530	82	0	0	5	0	2	2	8	0		1	99
$16a_g$	−9.034	8	71	0	11	2	0	0	6	0			
$11b_g$	−9.068	2	78	6	7	0	1	0	6	0			
$15a_g$	−9.263	17	36	2	18	10	8	2	8	0	2	5	93
$14b_u$	−9.941	14	0	3	25	13	31	5	10	1	17	19	64
$10b_g$	−10.180	11	0	3	30	26	19	3	9	0		20	80
$10a_u$	−10.255	14	0	2	28	1	30	6	11	0		18	82
$14a_g$	−10.352	21	16	6	8	1	30	6	11	0	16	12	72
$13b_u$	−10.736	5	0	2	29	47	6	1	10	0			
$13a_g$	−10.867	7	3	1	7	68	2	1	11	0			
$9a_u$	−10.933	8	1	1	24	50	6	1	10	0			
$9b_g$	−11.052	2	1	20	64	1	3	0	9	0			
$8b_g$	−11.110	12	1	0	12	52	9	2	12	0		15	85
$8a_u$	−11.2163	0	0	0	77	2	5	1	11	0			
$12b_u$	−11.271	8	1	16	25	41	1	1	8	0			
$12a_g$	−11.439	8	2	19	10	49	4	1	8	0			
$7a_u$	−11.583	1	1	43	38	4	2	1	11	0			
$11b_u$	−11.596	7	0	27	35	12	6	2	10	0			
$10b_u$	−11.901	9	2	8	41	27	4	1	10	0			
$7b_g$	−12.202	20	3	32	20	0	12	5	8	0		1	99
$6a_u$	−12.395	4	3	35	39	1	3	3	11	0			
$11a_g$	−12.397	14	9	0	45	17	3	1	10	0		6	94
$9b_u$	−12.515	5	4	32	46	0	1	1	10	0			
$5a_u$	−12.687	30	0	1	48	0	1	4	6	0			100
$8b_u$	−12.877	11	3	24	47	0	3	1	10	0	33	6	61
$10a_g$	−12.947	9	12	0	62	1	3	1	12	0			
$6b_g$	−12.980	11	11	19	35	0	8	7	9	0		2	98
$9a_g$	−13.485	10	7	34	13	9	11	11	6	0	4	1	95
$7b_u$	−13.565	25	0	50	1	17	1	1	5	0	8	1	91
$8a_g$	−13.644	7	17	14	52	2	1	1	8	0			
$4a_u$	−13.700	2	0	3	1	0	47	46	1	0			
$5b_g$	−13.721	1	7	5	12	0	37	36	3	0			
$4b_g$	−13.888	4	27	1	52	0	6	5	4	0			
$6b_u$	−13.935	2	0	3	0	0	46	45	2	0			
$7a_g$	−13.993	5	3	14	6	1	34	33	4	0			
$6a_g$	−14.302	5	23	57	1	2	4	4	5	0			
$3b_g$	−15.507	3	0	0	0	0	53	44	0	0			
$3a_u$	−15.511	3	0	0	1	0	52	44	0	0			
$5b_u$	−15.834	2	0	0	0	0	53	44	0	0			
$5a_g$	−15.844	2	0	1	0	0	53	44	0	0			
$4b_u$	−22.659	1	0	0	0	29	42	28	0	0			
$4a_g$	−22.660	1	0	0	0	30	42	28	0	0			
$2a_u$	−22.704	1	0	0	0	0	60	40	0	0			
$2b_g$	−22.704	1	0	0	0	0	60	40	0	0			
$3b_u$	−22.824	1	0	1	2	55	25	16	0	0			
$3a_g$	−22.836	1	0	0	1	54	26	17	0	0			
$1a_u$	−23.529	1	1	0	94	0	0	0	4	0			
$2b_u$	−23.607	1	1	0	91	1	1	1	4	0			
$1b_g$	−23.690	1	3	0	93	0	0	0	3	0			
$2a_g$	−23.880	1	3	5	87	0	0	0	4	0			
$1b_u$	−24.264	2	0	92	0	1	0	0	4	0			
$1a_g$	−24.531	2	2	87	4	1	0	0	4	0			

[a] The HOMO is the $16b_u$ orbital. [b] Results were rounded off to the nearest integral value; Ru_2 is the central Ru atom; Ru_1 refers to the peripheral Ru atoms. [c] Listed only for levels with at least 10% contribution from Ru atoms.

or diethyl ether. Large, dark red crystals, which were later characterized by X-ray crystallography as $Ru_2Cl_5(PMe_2Ph)_4$,[1] formed within 2–3 days. Tiny, needlelike green crystals also formed and were noticeable only under the microscope. These were determined to be those of $Ru_3Cl_8(PMe_2Ph)_4$ based on the electronic absorption spectrum (i.e., the presence of a maximum at 840 nm.).[4] Unfortunately, these crystals were not of sufficient quality to be studied by X-ray crystallography. The yield for $Ru_2Cl_5(PMe_2Ph)_4$ was substantially higher than that for compound **2**, although it was not measured for the latter.

Preparation of $Ru_3Cl_8(PEt_3)_4$ (3). A 0.61-g (2.33-mmol) sample of $RuCl_3 \cdot 3H_2O$ was dissolved in 2.5 mL of methanol, and then 0.37 g (3.11 mmol) of PEt_3 was added. The reaction mixture was stirred for 2 h and left undisturbed. After 8 days, dark blue-green crystals had deposited. These were recovered by filtration in air, washed with methanol (2 × 5 mL), and dried either in air or under vacuum. Yields varied between 31% and 51%. No dinuclear species was detected in the crude product even after recrystallization from CH_2Cl_2 using *n*-hexane as crystallizing solvent. The electronic absorption spectrum had maxima at 335, 480,

$Ru_3Cl_8(PH_3)_4$ $15b_u$ orbital

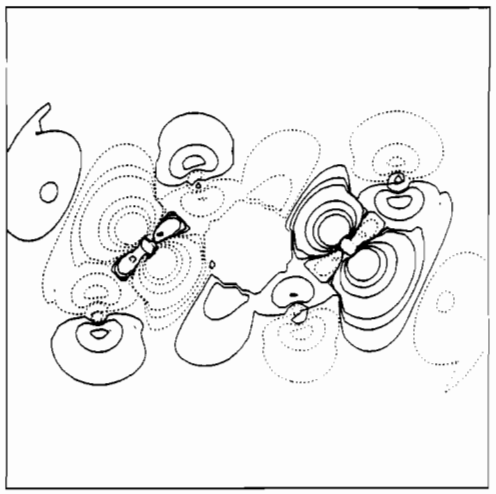

Figure 5. Contour plot of the $15b_u$ MO of $Ru_3Cl_8(PH_3)_4$. (by SCF–Xα–SW).

$Ru_3Cl_8(PH_3)_4$ $16a_g$ orbital

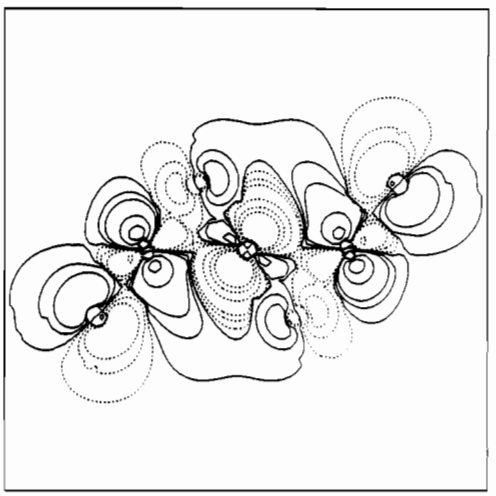

Figure 6. Contour plot of the $16a_g$ MO of $Ru_3Cl_8(PH_3)_4$. (by SCF–Xα–SW).

$Ru_3Cl_8(PH_3)_4$ $11b_g$ orbital

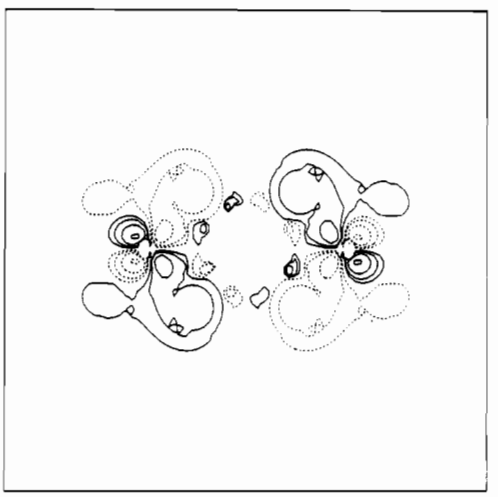

Figure 7. Contour plot of the $11b_g$ MO of $Ru_3Cl_8(PH_3)_4$. (by SCF–Xα–SW).

$Ru_3Cl_8(PH_3)_4$ $15a_g$ orbital

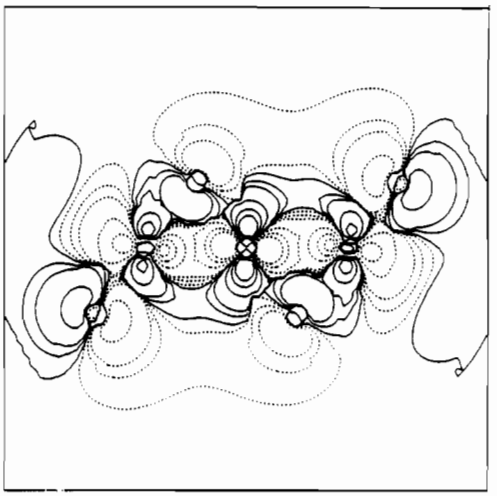

Figure 8. Contour plot of the $15a_g$ MO of $Ru_3Cl_8(PH_3)_4$. (by SCF–Xα–SW).

600, and 830–860 nm. ^{31}P NMR chemical shift: 21.63 ppm (singlet).

Preparation of $Ru_3Cl_8(PMe_3)_4$ (4a). The synthesis of $Ru_3Cl_8(PMe_3)_4$ was the same as that for the corresponding PEt_3 compound. A 0.24-g (3.11-mmol) sample of PMe_3 was added to 0.61 g (2.33 mmol) of $RuCl_3 \cdot 3H_2O$. The crude product, after recrystallization, was found to have no more than 4% of $Ru_2Cl_5(PMe_3)_4$[1] in most of the trials that were carried out. Yields for compound **4a** varied between 38% and 56%. Recrystallization was done by layering a CH_2Cl_2 solution of the crude product with 2–3 times its volume of benzene. Compound **4a** was determined to cocrystallize with one C_6H_6 molecule to give $Ru_3Cl_8(PMe_3)_4 \cdot C_6H_6$ (**4b**). $Ru_3Cl_8(PMe_3)_4$ was obtained in essentially pure form whenever PMe_3 was added very slowly (ca. 0.02 mL/min). In one instance where the phosphine ligand was accidentally added at a much faster rate, the amount of the diruthenium species present was correspondingly much higher than that in other trials. This was evident in the electronic absorption spectrum (maxima at 340, 420, 480, 570, and 800 nm). ^{31}P NMR chemical shift of $Ru_3Cl_8(PMe_3)_4$: 8.30 ppm (singlet).

Reaction of $Ru_3Cl_8(PR_3)_4$ [R = Et (3), Me (4), Bu (1)] with $AgSbF_6$. (a) R = Et. $[Ru_3Cl_8(PEt_3)_4][SbF_6]$ (**5**) was obtained by reacting 0.1 g (0.11 mmol) of $Ru_3Cl_8(PEt_3)_4$ and 0.038 g (0.11 mmol) of $AgSbF_6$ in 10 mL of CH_2Cl_2 or benzene and stirring at room temperature (ca. 25 °C) for 24 h. The solution turned from dark blue-violet to dark red-violet. It was then slowly layered with 25 mL of *n*-hexane. Within 5 days, dark red-violet crystals formed. The product weighed 0.10 g (0.077 mmol; 77% yield). The electronic absorption spectrum had maxima at 290–300 nm ($\epsilon = 8.22 \times 10^3$ cm^{-1} M^{-1}), 365 nm ($\epsilon = 5.37 \times 10^3$ cm^{-1} M^{-1}; shoulder at 420 nm), 515 nm ($\epsilon = 5.20 \times 10^3$ cm^{-1} M^{-1}), and 780 nm ($\epsilon = 2.17 \times 10^3$ cm^{-1} M^{-1}). A crystal from the deposited product was good enough for X-ray structure determination and was determined to be indeed $[Ru_3Cl_8(PEt_3)_4][SbF_6]$.

(b) R = Me. $[Ru_3Cl_8(PMe_3)_4][SbF_6]$ (**6**) was obtained as in part a. A 0.05-g (0.056-mmol) sample of $Ru_3Cl_8(PMe_3)_4$ and 0.02 g (0.058 mmol) of $AgSbF_6$ were used. The solution turned from dark blue-violet to red-violet in 24 h. This was layered with *n*-hexane, and within 2 weeks, tiny dark red-violet crystals formed and 0.020 g (0.018 mmol, 32% yield) of product was recovered by filtration in air. The electronic absorption spectrum had maxima at 280–300, 370, 520, and 800 nm.

(c) R = Bu. $[Ru_3Cl_8(PBu_3)_4][SbF_6]$ (**7**) was prepared as in part a by using 0.1 g (0.07 mmol) of the triruthenium complex and 0.03 g (0.085 mmol) of $AgSbF_6$ as starting materials. The solution turned dark red-violet within 24 h. This was layered with *n*-hexane to give a dark red-violet precipitate within 5 days. The product was identified by comparing the electronic absorption spectrum (maxima at 300, 420, 570, and 830 nm) with those in parts a and b.

Reactions of $Ru_3Cl_8(PR_3)_4$ [R = Et (3), Bu (1)] with Cp_2Co. (a) R = Et. A 0.1-g (0.09-mmol) sample of $Ru_3Cl_8(PEt_3)_4$ and 0.020 g (0.11 mmol) of Cp_2Co were reacted in 10 mL of benzene or THF. The solution turned from dark violet to dark green within 3 min. This was layered with 25 mL of *n*-hexane and left undisturbed. A brownish green precipitate deposited within 2 days. The yield, though not measured, was low. The electronic absorption spectrum had maxima at 380 nm (very broad) and at 800 nm (broad). These peaks are virtually the same as those for "Ru_3^{7+}"-containing cationic trimers, $[Ru_3Cl_6(PR_3)_6]^+$ (R = Et, Bu),[7] and they indicate that $[Cp_2Co][Ru_3Cl_8(PEt_3)_4]$ (**8**) had been produced. This product appeared stable in the solid state. Using 2 equiv

Table VIII. Ru Contributions and Symmetry Correlations between MOs of $[Ru_3Cl_{12}]^{4-}$ and $Ru_3Cl_8(PH_3)_4$

	$[Ru_3Cl_{12}]^{4-}$, D_{3d}			$Ru_3Cl_8(PH_3)_4$, C_{2h}		
		% Ru			% Ru	
		Ru_c	Ru_t		Ru_c	Ru_t
LUMO	$8a_{1g}$	26	58	$18a_g$	28	58
HOMO	$7a_{2u}$	0	75	$16b_u$	0	78
	$9e_u$	0	75	$11a_u$	0	79
				$15b_u$	0	82
	$10e_g$	1	73	$12b_g$	1	78
				$17a_g$	6	76
	$9e_g$	72	2	$16a_g$	71	8
				$11b_g$	78	2
	$7a_{1g}$	37	12	$15a_g$	36	17

[a] Ru_c = central ruthenium atom; Ru_t = outer ruthenium atoms.

Table IX. Selected Electronic Transitions for $Ru_3Cl_8(PH_3)_4$

		calcd energy	
orbital transition	type[a]	E, eV	E, cm^{-1}
$16b_u \rightarrow 18a_g$	a	0.580	4640
$11a_u \rightarrow 18a_g$	a	0.630	5040
$12b_g \rightarrow 18a_g$	f	0.623	4984
$17a_g \rightarrow 18a_g$	f	0.791	6328
$15b_u \rightarrow 18a_g$	a	0.748	5984
$16a_g \rightarrow 18a_g$	f	1.501	12008
$11b_g \rightarrow 18a_g$	f	1.608	12864
$15a_g \rightarrow 18a_g$	f	1.576	12608

[a] a = electric-dipole allowed; f = electric-dipole forbidden.

(0.040 g, 0.22 mmol) of the reductant, Cp_2Co, instead of 1 equiv immediately gave a rose-colored solid and an orange-brown benzene or THF solution. When exposed to air, the mixture proved to be extremely sensitive, turning brownish green within a minute. The brownish green material had the same electronic absorption spectrum and exhibited the same behavior as compound **8**.

(b) R = Bu. The reaction of $Ru_3Cl_8(PBu_3)_4$ (0.1 g, 0.07 mmol) with 1 (0.015 g, 0.08 mmol) or 2 equiv of Cp_2Co in benzene or THF behaved in the same way as the reactions involving the corresponding PEt_3 complex. The electronic absorption of $[Cp_2Co][Ru_3Cl_8(PBu_3)_4]$ (**9**) had maxima at 380 nm (very broad) and 820 nm (broad).

Reactions of $Ru_3Cl_8(PBu_3)_4$ (1) with Na/Hg. $Ru_3Cl_8(PBu_3)_4$ (0.1 g, 0.07 mmol) was dissolved in benzene, toluene, or THF, and 1 equiv Na/Hg amalgam was added while the solution was being stirred. The dark violet solution turned brownish green in less than 5 min. This was filtered through Celite into a Schlenk tube containing Ph_4AsCl. The solution was layered with *n*-hexane and left undisturbed. Within 1 week, a dull green solid precipitated and was harvested by filtration. This was found to be stable in CH_2Cl_2 and in air. The yield, however, was very low. The electronic absorption spectrum had maxima at 360 nm (broad) and 820 (broad), indicating that the starting material was most probably reduced to $[Ru_3Cl_8(PBu_3)_4]^-$. Other counterions such as Ph_4P^+ and PPN^+ gave similar results as Ph_4As^+ and likewise failed to give crystals suitable for X-ray structure determination. Using 2 equiv of Na/Hg amalgam gave an orange-brown solution. This was treated similarly and yielded brown crystals within 1 week. However, the product was extremely air-sensitive and the crystals decomposed during both isolation procedures and crystal mounting for an X-ray diffraction experiment. Repeated attempts to crystallize the complex in the brown solution, even with different counterions (Ph_4P^+, PPN^+, and 15-crown-5 to form $[Na\{15\text{-crown-}5\}]^+$), were unsuccessful.

X-ray Crystallography. The structure determination for each compound was carried out by employing procedures routine in this laboratory.[8] Pertinent crystallographic data and refinement results are listed in Tables I and II. The final thermal displacement parameters, together with full tables of bond distances and angles, are available in the supplementary material.

For **3**, initial examination showed that the crystal system was monoclinic with a primitive lattice. Oscillation photographs confirmed this and the Laue group ($2/m$). Systematic absences observed were unique for space group $P2_1/n$. The heavy atoms were found by direct methods and were consistent with the determined space group. An alternating series of Fourier maps and least-squares refinement cycles revealed the location of the other non-hydrogen atoms. After the model refined satisfactorily with all the atoms having anisotropic thermal displacement parameters, hydrogen atoms were added in calculated positions. The model was allowed to refine with the methylenic hydrogen atoms constrained to have the same isotropic thermal displacement parameter; methyl hydrogen atoms were also constrained to have the same isotropic thermal displacement parameter. Table III lists the final positional and isotropic equivalent thermal displacement parameters.

For **4a**, preliminary examination revealed that the crystal system was monoclinic with a primitive lattice. These and the Laue group ($2/m$) were confirmed by oscillation photographs. Systematic conditions observed were unique for space group $P2_1/n$. The heavy atoms were found by using direct methods and were consistent with this space group. The rest of the non-hydrogen atoms were located by an alternating series of Fourier maps and least-squares refinement cycles. Hydrogen atoms were not included in the model. Table IV lists the final positional and isotropic equivalent thermal displacement parameters.

For **4b**, preliminary examination showed that the crystal system was triclinic and oscillation photographs confirmed this and the Laue group ($\bar{1}$). The heavy atoms were found by direct methods and were consistent

$Ru_3Cl_8(PH_3)_4$ $18a_g$ orbital

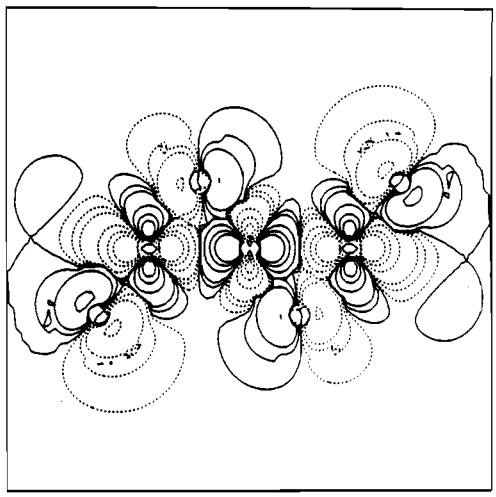

Figure 9. Contour plot of the $18a_g$ MO of $Ru_3Cl_8(PH_3)_4$, the LUMO. (by SCF-Xα-SW).

$Ru_3Cl_8(PH_3)_4$ $14a_g$ orbital

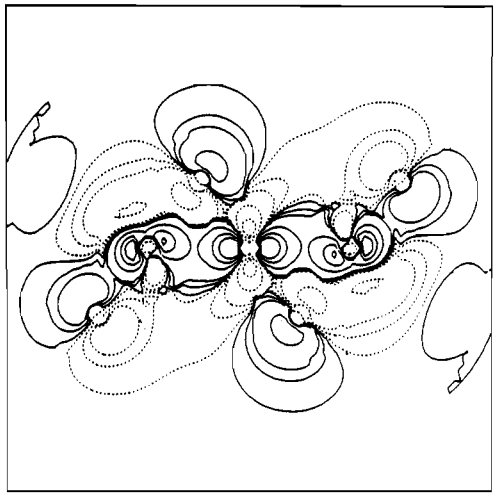

Figure 10. Contour plot of the $14a_g$ MO of $Ru_3Cl_8(PH_3)_4$. (by SCF-Xα-SW).

(7) These compounds are discussed in a separate paper (Part 4 of this series).

(8) The calculations were done on a MicroVax II computer with an SDP package software. ψ-Scan absorption corrections were made by following: North, A. C. T.; Phillips, D. C.; Matthews, F. S. *Acta Crystallogr.* **1968**, *A24*, 351. Structure solutions employed: Sheldrick, G. M. SHELXS-86. Institut fur Anorganische Chemie der Universitat, Göttingen, FRG, 1986. Sheldrick, G. M. SHELX-76. Program for Crystal Structure Determination. University of Cambridge, Cambridge, England, 1976.

Table X. Molecular Orbitals of $Ru_3Cl_8(PH_3)_4$ from Fenske–Hall Calculations

levels[a]	energy, eV	% contribn[b]						% angular contribn[c]					
								Ru_c			Ru_t		
		Ru_c	Ru_t	Cl_b	Cl_t	P	H	s	p	d	s	p	d
$17b_u$	1.89	2	62	16	14	5	0		4			8	88
$12a_u$	1.54	2	64	19	0	14	0		4			21	75
$19a_g$	0.29	33	30	28	7	2	0			52		7	41
$13b_g$	0.14	28	36	28	0	7	0			44		16	40
$18a_g$	−4.44	44	41	12	2	0	0			51			49
$16b_u$ (HOMO)	−6.76	0	75	10	14	0	0						100
$12b_g$	−6.77	19	54	16	11	0	0			27			73
$17a_g$	−6.92	57	17	26	0	0	0			77			23
$11a_u$	−6.97	0	74	6	19	0	0						100
$11b_g$	−7.49	59	25	8	7	0	0			70			30
$16a_g$	−7.77	20	61	4	14	0	1			27			73
$15b_u$	−7.82	0	87	10	0	1	2						100
$15a_g$	−8.80	22	40	14	21	2	1			35			65
$14b_u$	−9.96	1	5	27	64	2	1						
$10b_g$	−10.11	2	10	28	56	3	1			13		17	70
$10a_u$	−10.34	0	12	20	65	2	1					7	93
$14a_g$	−10.91	8	22	9	60	0	1	1		26	1	1	71
$9b_g$	−10.95	0	1	90	9	0	0						
$9a_u$	−11.23	4	6	79	9	1	1		44			5	51
$13a_g$	−11.24	1	14	31	52	1	1			4	4	50	42
$13b_u$	−11.26	2	9	56	30	2	1		16		5	39	40
$12b_u$	−11.52	0	14	43	39	2	2		2			46	51
$8a_u$	−11.97	1	0	97	0	1	1						
$8b_g$	−12.14	0	16	62	15	6	1			2		25	73
$11b_u$	−12.34	3	13	60	13	1	0		19		6	12	63
$12a_g$	−12.75	10	18	44	23	4	1			36	2	11	50
$7a_u$	−12.90	0	12	80	2	6	0					40	60
$10b_u$	−13.31	3	11	83	2	1	0			23	2	5	70
$6a_u$	−13.68	2	8	85	3	1	1			18		5	76
$9b_u$	−13.89	5	6	87	0	1	1		42		2	2	54
$11a_g$	−14.29	21	9	60	3	6	1	1		68	1	12	17
$8b_u$	−14.54	0	23	71	6	0	0				6	6	88
$10a_g$	−14.72	21	6	72	0	0	0	23		56			21
$7b_g$	−14.78	29	8	58	0	4	1			80			20
$6b_g$	−14.92	20	4	72	0	2	1			83			16
$9a_g$	−15.02	14	14	67	1	3	1	11		38		3	48
$8a_g$	−15.55	25	3	71	0	1	0	8		80	1		11
$5a_u$	−15.64	0	36	8	0	50	5					10	90
$5b_g$	−15.67	3	32	12	1	47	5			9		11	80
$7b_u$	−17.04	0	18	11	2	63	6				53	9	38
$7a_g$	−17.21	3	15	19	2	55	6	6		10	51	7	26
$4a_u$	−21.10	0	0	0	0	43	56						
$4b_g$	−21.10	0	0	0	0	43	56						
$6b_u$	−21.36	0	0	1	1	44	53						
$6a_g$	−21.37	0	0	1	1	44	53						
$3a_u$	−21.55	0	0	0	0	43	56						
$3b_g$	−21.56	0	0	0	0	43	56						
$5a_g$	−22.26	0	0	0	0	48	56						
$5b_u$	−22.26	0	0	0	0	48	51						
$4a_g$	−25.52	2	0	0	95	2	0						
$4b_u$	−25.52	2	0	0	95	2	0						
$3b_u$	−27.14	0	1	98	0	1	0						
$2a_u$	−27.17	0	2	98	0	0	0						
$3a_g$	−27.37	3	0	95	0	1	0						
$2b_g$	−27.66	6	1	92	0	0	0						
$2b_u$	−28.18	0	2	97	0	1	0						
$2a_g$	−28.55	5	1	92	0	1	0						
$1a_g$	−29.01	0	0	0	0	60	39						
$1b_u$	−29.01	0	0	0	0	60	39						
$1a_u$	−29.02	0	0	0	0	60	39						
$1b_g$	−29.02	0	0	0	0	60	39						

[a] The HOMO is the $16b_u$ orbital. [b] Results were rounded off to the nearest integral value; Ru_c is the central Ru atom; Ru_t refers to the peripheral Ru atoms; Cl_b and Cl_t refer to the bridging and terminal Cl atoms, respectively. [c] Listed only for levels with at least 10% contribution from Ru atoms.

with space group $P\bar{1}$. $P\bar{1}$ was assumed (in preference to $P1$) and allowed for satisfactory refinement. The rest of the non-hydrogen atoms were located by an alternating series of Fourier maps and least-squares refinement cycles. After all the non-hydrogen atoms refined to convergence with anisotropic thermal displacement parameters, hydrogen atoms were added in calculated positions. The model was allowed to refine with the methyl hydrogen atoms constrained to have the same isotropic thermal displacement parameter; phenyl hydrogens were also constrained to have the same isotropic thermal displacement parameter. Table V lists the final positional and isotropic equivalent thermal displacement parameters.

For **5**, initial examination showed that the crystal system was monoclinic with a primitive lattice. This observation and the Laue group $(2/m)$ were confirmed by oscillation photographs. Systematic absences observed were unique for space group $P2_1/a$. The positions of all the ruthenium atoms and one antimony atom (which was lying on a center of inversion) were found by direct methods and were consistent with the determined space group. The remaining Sb atom and the rest of the non-hydrogen atoms were located by an alternating series of Fourier maps and least-squares refinement cycles. Two independent pairs of cations were determined to be present in the asymmetric unit. One

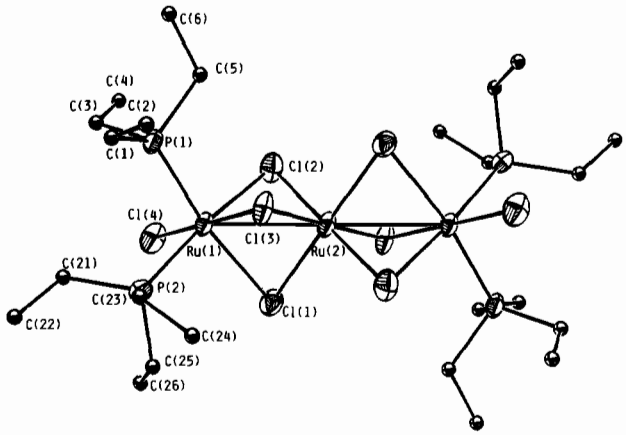

Figure 11. ORTEP drawing of the $Ru_3Cl_8(PEt_3)_4$ molecule (**3**). Ru(2) is on a crystallographic center of inversion which relates each unlabeled atom to a labeled one. Carbon atoms were given arbitrary radii.

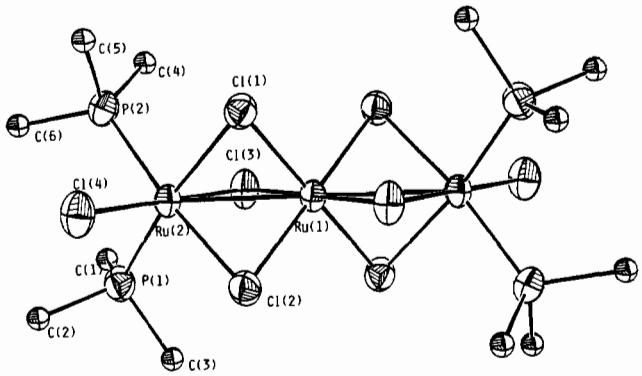

Figure 12. ORTEP drawing of the $Ru_3Cl_8(PMe_3)_4$ molecule (**4**). Ru(1) is on a crystallographic center of inversion which relates each unlabeled atom to a labeled one. Carbon atoms were given arbitrary radii.

cation/anion set was lying on general positions while the other set had the cation and anion each lying on a center of inversion. The C–C distances in the ethyl groups of the cation lying on a general position were unrealistically long until they were constrained to correspond to 1.5 Å. Table VI lists the final positional and isotropic equivalent thermal displacement parameters.

Theoretical Calculations. Molecular orbital calculations employing the Fenske–Hall[9] and SCF-Xα-SW[10] methods were done for $Ru_3Cl_8(PR_3)_4$. Atomic coordinates used in both calculations were based on the X-ray structural data for $Ru_3Cl_8(PBu_3)_4$[4] and were idealized to C_{2h} symmetry. In the model, the butyl chains were replaced by hydrogen atoms. The coordinate system was set with the origin at the center of the molecule (i.e., the central Ru atom), the z axis was directed along the Ru–Ru vector, and the y axis contained the principal axis.

Fenske–Hall Calculations. The basis functions used for Ru were taken from Richardson[11] and were augmented by 5s and 5p atomic orbitals each with an exponent of 2.20. Slater type orbitals (STOs) were utilized for Cl, P, and H atoms.[12] A value of 1.20 was used as the exponent for hydrogen atoms. The individual atomic charges were determined by using the Mulliken population analysis.

SCF-Xα-SW Calculations. This method employed a slightly modified program, which was created by M. Cook (Harvard University). Initial molecular potentials were obtained from a superposition of Herman–Skillman atomic potentials. The α values for the atoms involved were taken from a tabulation by Schwarz.[13] For the inter- and outer-sphere regions, a valence-electron weighted average of the atomic α values was used. Sphere radii were chosen based on Norman's procedure[14] and were chosen as 89% of the atomic number radii. The atomic spheres were allowed to overlap. The outer-sphere radius was made tangential to the outermost atomic sphere. The SCF calculations were considered to be converged when the shift in potential was less than 0.001 Rydberg. No relativistic correction was employed.

Table XI. Selected Bond Distances (Å) and Angles (deg) for $Ru_3Cl_8(PEt_3)_4$ (**3**)[a]

Bond Distances			
Ru(1)–Ru(2)	2.862 (1)	Ru(2)–Cl(2)	2.474 (5)
Ru(1)–Cl(1)	2.375 (4)	Ru(2)–Cl(3)	2.367 (4)
Ru(1)–Cl(2)	2.366 (5)	Ru(2)–Cl(4)	2.338 (4)
Ru(1)–Cl(3)	2.356 (4)	Ru(2)–P(1)	2.323 (4)
Ru(2)–Cl(1)	2.501 (4)	Ru(2)–P(2)	2.328 (5)
Bond Angles			
Ru(2)–Ru(1)–Ru(2′)	180.00 (0)	Ru(1)–Ru(2)–P(1)	119.4 (1)
Ru(2)–Ru(1)–Cl(1)	56.12 (9)	Ru(1)–Ru(2)–P(2)	125.1 (1)
Ru(2)–Ru(1)–Cl(2)	55.5 (1)	Cl(1)–Ru(2)–Cl(2)	83.0 (2)
Ru(2)–Ru(1)–Cl(3)	52.87 (9)	Cl(1)–Ru(2)–Cl(3)	86.9 (1)
Ru(2)–Ru(1)–Cl(1′)	123.88 (9)	Cl(1)–Ru(2)–Cl(4)	92.3 (1)
Ru(2)–Ru(1)–Cl(2′)	124.5 (1)	Cl(1)–Ru(2)–P(1)	171.4 (2)
Ru(2)–Ru(1)–Cl(3′)	127.13 (9)	Cl(1)–Ru(2)–P(2)	90.5 (2)
Cl(1)–Ru(1)–Cl(1′)	180.00 (0)	Cl(2)–Ru(2)–Cl(3)	89.0 (1)
Cl(1)–Ru(1)–Cl(2)	88.1 (2)	Cl(2)–Ru(2)–Cl(4)	89.7 (2)
Cl(1)–Ru(1)–Cl(2′)	91.9 (2)	Cl(2)–Ru(2)–P(1)	90.7 (2)
Cl(1)–Ru(1)–Cl(3)	90.1 (1)	Cl(2)–Ru(2)–P(2)	172.6 (2)
Cl(1)–Ru(1)–Cl(3′)	89.9 (1)	Cl(3)–Ru(2)–Cl(4)	178.6 (2)
Cl(2)–Ru(1)–Cl(2′)	180.00 (0)	Cl(3)–Ru(2)–P(1)	87.1 (1)
Cl(2)–Ru(1)–Cl(3)	91.9 (1)	Cl(3)–Ru(2)–P(2)	94.4 (2)
Cl(2)–Ru(1)–Cl(3′)	88.1 (1)	Cl(4)–Ru(2)–P(1)	93.6 (2)
Cl(3)–Ru(1)–Cl(3′)	180.00 (0)	Cl(4)–Ru(2)–P(2)	86.8 (2)
Ru(1)–Ru(2)–Cl(1)	52.0 (1)	P(1)–Ru(2)–P(2)	96.0 (2)
Ru(1)–Ru(2)–Cl(2)	52.0 (1)	Ru(1)–Cl(1)–Ru(2)	71.8 (1)
Ru(1)–Ru(2)–Cl(3)	52.53 (9)	Ru(1)–Cl(2)–Ru(2)	72.5 (1)
Ru(1)–Ru(2)–Cl(4)	126.1 (1)	Ru(1)–Cl(3)–Ru(2)	74.6 (1)

[a] Numbers in parentheses are estimated standard deviations in the least significant digits.

Table XII. Selected Bond Distances (Å) and Angles (deg) for $Ru_3Cl_8(PMe_3)_4$ (**4a**)[a]

Bond Distances			
Ru(1)–Ru(2)	2.828 (1)	Ru(2)–Cl(2)	2.503 (2)
Ru(1)–Cl(1)	2.360 (2)	Ru(2)–Cl(3)	2.375 (3)
Ru(1)–Cl(2)	2.374 (3)	Ru(2)–Cl(4)	2.348 (3)
Ru(1)–Cl(3)	2.356 (2)	Ru(2)–P(1)	2.305 (3)
Ru(2)–Cl(1)	2.450 (3)	Ru(2)–P(2)	2.301 (2)
Bond Angles			
Ru(2)–Ru(1)–Ru(2′)	180.00 (0)	Ru(1)–Ru(2)–P(1)	122.68 (6)
Ru(2)–Ru(1)–Cl(1)	55.49 (6)	Ru(1)–Ru(2)–P(2)	118.79 (8)
Ru(2)–Ru(1)–Cl(2)	56.72 (5)	Cl(1)–Ru(2)–Cl(2)	83.40 (8)
Ru(2)–Ru(1)–Cl(3)	53.61 (6)	Cl(1)–Ru(2)–Cl(3)	90.08 (9)
Ru(2)–Ru(1)–Cl(1′)	124.51 (6)	Cl(1)–Ru(2)–Cl(4)	91.92 (9)
Ru(2)–Ru(1)–Cl(2′)	123.28 (5)	Cl(1)–Ru(2)–P(1)	169.90 (8)
Ru(2)–Ru(1)–Cl(3′)	126.39 (6)	Cl(1)–Ru(2)–P(2)	90.95 (9)
Cl(1)–Ru(1)–Cl(1′)	180.00 (0)	Cl(2)–Ru(2)–Cl(3)	87.38 (8)
Cl(1)–Ru(1)–Cl(2)	88.24 (8)	Cl(2)–Ru(2)–Cl(4)	95.26 (8)
Cl(1)–Ru(1)–Cl(2′)	91.76 (8)	Cl(2)–Ru(2)–P(1)	87.00 (8)
Cl(1)–Ru(1)–Cl(3)	87.19 (8)	Cl(2)–Ru(2)–P(2)	171.2 (1)
Cl(1)–Ru(1)–Cl(3′)	92.81 (8)	Cl(3)–Ru(2)–Cl(4)	176.85 (9)
Cl(2)–Ru(1)–Cl(2′)	180.00 (0)	Cl(3)–Ru(2)–P(1)	92.58 (9)
Cl(2)–Ru(1)–Cl(3)	89.08 (9)	Cl(3)–Ru(2)–P(2)	85.93 (9)
Cl(2)–Ru(1)–Cl(3′)	90.92 (9)	Cl(4)–Ru(2)–P(1)	85.9 (1)
Cl(3)–Ru(1)–Cl(3′)	180.00 (0)	Cl(4)–Ru(2)–P(2)	91.61 (9)
Ru(1)–Ru(2)–Cl(1)	52.52 (5)	P(1)–Ru(2)–P(2)	99.0 (1)
Ru(1)–Ru(2)–Cl(2)	52.45 (6)	Ru(1)–Cl(1)–Ru(2)	71.99 (7)
Ru(1)–Ru(2)–Cl(3)	52.97 (6)	Ru(1)–Cl(2)–Ru(2)	70.83 (6)
Ru(1)–Ru(2)–Cl(4)	130.13 (7)	Ru(1)–Cl(3)–Ru(2)	73.43 (7)

[a] Numbers in parentheses are estimated standard deviations in the least significant digits.

(9) Fenske, R. E.; Hall, M. B. *Inorg. Chem.* **1972**, *11*, 768.
(10) (a) Johnson, K. H. *Annu. Rev. Phys. Chem.* **1975**, *26*, 39. (b) Slater, J. C. *Quantum Theory as Molecules and Solids*; McGraw-Hill: New York, 1974. (c) Cotton, F. A.; Hubbard, J. L.; Lichtenberger, D. L.; Shim, I. *J. Am. Chem. Soc.* **1982**, *104*, 679.
(11) Richardson, J. W.; Blackman, M. J.; Ranochak, J. E. *J. Chem. Phys.* **1973**, *58*, 3010.
(12) Tables of Atomic Functions. A supplement to a paper by Clementi: Clementi, E. *IBM J. Res. Dev.* **1965**, 912.
(13) (a) Schwarz, K. *Phys. Rev. B.*, **1971**, *5*, 2466. (b) Schwarz, K. *Theor. Chim. Acta* **1974**, *34*, 225.
(14) Norman, J. G., Jr. *Mol. Phys.* **1976**, *31*, 1191.

Table XIII. Selected Bond Distances (Å) and Angles (deg) for $Ru_3Cl_8(PMe_3)_4 \cdot C_6H_6$ (**4b**)[a]

Bond Distances			
Ru(1)–Ru(2)	2.842 (0)	Ru(2)–Cl(2)	2.482 (1)
Ru(1)–Cl(1)	2.358 (1)	Ru(2)–Cl(3)	2.483 (1)
Ru(1)–Cl(2)	2.369 (1)	Ru(2)–Cl(4)	2.348 (1)
Ru(1)–Cl(3)	2.371 (1)	Ru(2)–P(1)	2.310 (1)
Ru(2)–Cl(1)	2.377 (1)	Ru(2)–P(2)	2.307 (1)
Bond Angles			
Ru(2)–Ru(1)–Ru(2′)	180.00 (0)	Ru(1)–Ru(2)–P(1)	121.72 (2)
Ru(2)–Ru(1)–Cl(1)	53.41 (1)	Ru(1)–Ru(2)–P(2)	120.72 (2)
Ru(2)–Ru(1)–Cl(2)	56.00 (2)	Cl(1)–Ru(2)–Cl(2)	88.62 (2)
Ru(2)–Ru(1)–Cl(3)	56.01 (2)	Cl(1)–Ru(2)–Cl(3)	87.97 (2)
Ru(2)–Ru(1)–Cl(1′)	126.59 (1)	Cl(1)–Ru(2)–Cl(4)	177.95 (3)
Ru(2)–Ru(1)–Cl(2′)	124.00 (2)	Cl(1)–Ru(2)–P(1)	87.14 (2)
Ru(2)–Ru(1)–Cl(3′)	123.99 (2)	Cl(1)–Ru(2)–P(2)	92.25 (2)
Cl(1)–Ru(1)–Cl(1′)	180.00 (0)	Cl(2)–Ru(2)–Cl(3)	83.64 (2)
Cl(1)–Ru(1)–Cl(2)	88.19 (2)	Cl(2)–Ru(2)–Cl(4)	93.42 (2)
Cl(1)–Ru(1)–Cl(2′)	91.81 (2)	Cl(2)–Ru(2)–P(1)	174.02 (2)
Cl(1)–Ru(1)–Cl(3)	88.90 (2)	Cl(2)–Ru(2)–P(2)	86.33 (2)
Cl(1)–Ru(1)–Cl(3′)	91.10 (2)	Cl(3)–Ru(2)–Cl(4)	92.26 (2)
Cl(2)–Ru(1)–Cl(2′)	180.00 (0)	Cl(3)–Ru(2)–P(1)	91.98 (3)
Cl(2)–Ru(1)–Cl(3)	88.61 (2)	Cl(3)–Ru(2)–P(2)	169.96 (2)
Cl(2)–Ru(1)–Cl(3′)	91.39 (2)	Cl(4)–Ru(2)–P(1)	90.82 (3)
Cl(3)–Ru(1)–Cl(3′)	180.00 (0)	Cl(4)–Ru(2)–P(2)	87.87 (2)
Ru(1)–Ru(2)–Cl(1)	52.81 (2)	P(1)–Ru(2)–P(2)	98.06 (3)
Ru(1)–Ru(2)–Cl(2)	52.30 (1)	Ru(1)–Cl(1)–Ru(2)	73.78 (2)
Ru(1)–Ru(2)–Cl(3)	52.35 (2)	Ru(1)–Cl(2)–Ru(2)	71.70 (2)
Ru(1)–Ru(2)–Cl(4)	128.71 (2)	Ru(1)–Cl(3)–Ru(2)	71.64 (2)

[a] Numbers in parentheses are estimated standard deviations in the least significant digits.

Table XIV. Selected Structural Parameters for Linear Trinuclear Ru Complexes with Octahedra Joined on Faces

	Ru–Ru, Å	α_1,[a] deg	α_2,[b] deg	β,[c] deg
$Ru_3Cl_8(PR_3)_4$				
R = Bu	2.85	86.4	88.2	73.0
R = Et	2.86	86.3	90.0	73.0
R = Me	2.83	87.0	88.2	72.1
$Ru_3Cl_8(PMe_3)_4 \cdot C_6H_6$	2.84	86.7	91.6	72.4
$[Ru_3Cl_{12}]^{4-}$	2.81	88.5	88.9	72.4
$[Ru_3Cl_8(PEt_3)_4][SbF_6]$	2.91	84.9	89.3	74.5

[a] $\alpha_1 = \angle Cl_b–Ru_t–Cl_b$. [b] $\alpha_2 = \angle Cl_b–Ru_c–Cl_b$. [c] $\beta = \angle Ru–Cl_b–Ru$.

Results and Discussion

Although it is the experimental results that are of paramount importance, it is expedient to give the results of the electronic structure analysis first since these provide a very useful framework within which to organize the rest of the discussion.

The pertinent results of the molecular orbital calculations for the model compound, $Ru_3Cl_8(PH_3)_4$, using the SCF–Xα–SW method are summarized in Table VII, which lists the data for the upper valence MOs. Figures 1–8 are the plots of the eight highest occupied MOs. It is evident that these eight orbitals have predominantly metal atom d orbital character. The rest of the MOs, lying below these, having mainly chlorine or phosphorus 3p orbital character, and occupied by a total of 48 electron pairs, are Ru–Cl bonding, Cl lone-pair orbitals, Ru–P bonding, or P–H bonding orbitals. The ordering of the levels is not in complete agreement with the qualitative description put forth[2,3] because there a strict separation of the dπ and dδ orbitals was maintained. In fact, substantial mixing between the dπ and dδ sets occurs and this is responsible for the difference in the ordering of the molecular orbitals.

The $18a_g$ MO or lowest unoccupied molecular orbital, LUMO, shown in Figure 9, likewise has predominantly metal atom d orbital character. It is antibonding in nature with respect to metal–ligand and metal–metal σ bonding. The highest occupied molecular orbital, HOMO, shown in Figure 1, is $16b_u$ and it is essentially nonbonding as far as metal–metal σ bonding is concerned as the electron density is concentrated on the outer ruthenium atoms (having a major contribution from the d_{z^2} orbitals). The $11a_u$, $12b_g$, $17a_g$, and $15b_u$ orbitals are also essentially nonbonding as may be deduced from Figures 2–5. They are largely localized on the outer ruthenium atoms and are similar to one another. Likewise, the $16a_g$ and $11b_g$ orbitals, shown in Figures 6 and 7, are nonbonding in nature and are mainly concentrated on the central ruthenium atom. The metal–metal bonding is primarily σ bonding in nature, and the major contribution to this is provided by the $15a_g$ MO, shown in Figure 8, which consists primarily of the Ru d_{z^2} orbitals. A significant contribution also comes from the next lower a_g MO, $14a_g$, shown in Figure 10.

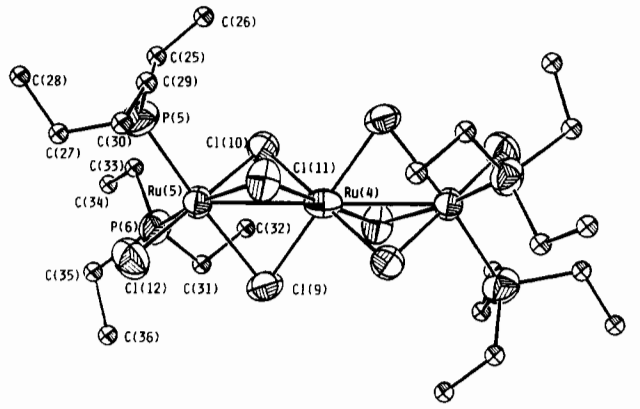

Figure 13. ORTEP drawing of the $[Ru_3Cl_8(PEt_3)_4]^+$ cation in compound **5** possessing C_{2h} symmetry. Carbon atoms were given arbitrary radii.

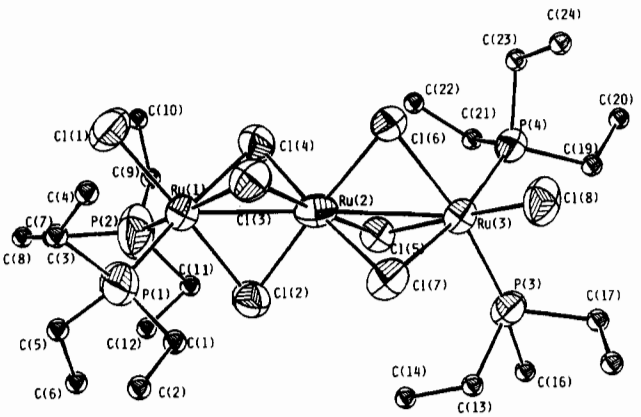

Figure 14. ORTEP drawing of the $[Ru_3Cl_8(PEt_3)_4]^+$ cation in compound **5** possessing C_2 symmetry. Carbon atoms were given arbitrary radii.

These results are very similar to those obtained for $[Ru_3Cl_{12}]^{4-}$.[3] There is good correspondence between the upper valence MOs of $[Ru_3Cl_{12}]^{4-}$ and $Ru_3Cl_8(PH_3)_4$ with regard to symmetry and to the percentage contribution of the metal atom d orbitals, as indeed there should be since the only differences between the two systems are the presence of the PH_3 groups in place of four of the Cl ligands and the interatomic distances. The higher energies in $Ru_3Cl_8(PH_3)_4$ may be attributed to the relatively larger energies (less negative energies) for the phosphorus atom basis orbitals. Table VIII illustrates the correspondence between the MOs of $[Ru_3Cl_{12}]^{4-}$ and $Ru_3Cl_8(PH_3)_4$.

In an effort to assign the intense near-infrared absorption band that is characteristic of the $Ru_3Cl_8(PR_3)_4$ compounds, several possible electronic transitions were considered and the corresponding excitation energies calculated in spin-restricted form for $Ru_3Cl_8(PH_3)_4$. The results are listed in Table IX. Three electric dipole forbidden transitions between 12000 and 13000 cm^{-1} come close to the observed broad band between 11900 and 12500 cm^{-1}. Two of these transitions, namely, $15a_g \rightarrow 18a_g$ and $16a_g \rightarrow 18a_g$, are transitions from the A_g ground state to an A_g excited state. The $11b_g \rightarrow 18a_g$ orbital transition corresponds to a transition from the A_g ground state to B_g. The $15a_g \rightarrow 18a_g$ orbital transition essentially corresponds to a forbidden $\sigma \rightarrow \sigma^*$ transition. The significant metal–ligand interaction in the $15a_g$ orbital implies

Table XV. Selected Bond Distances (Å) and Angles (deg) for $[Ru_2Cl_8(PEt_3)_4][SbF_6]$ (**5**)[a]

Bond Distances			
Ru(1)–Ru(2)	2.804 (3)	Ru(4)–Ru(5)	2.892 (2)
Ru(1)–Cl(1)	2.297 (7)	Ru(4)–Cl(9)	2.367 (6)
Ru(1)–Cl(2)	2.346 (6)	Ru(4)–Cl(10)	2.342 (6)
Ru(1)–Cl(3)	2.489 (7)	Ru(4)–Cl(11)	2.346 (6)
Ru(1)–Cl(4)	2.480 (7)	Ru(5)–Cl(9)	2.494 (6)
Ru(1)–P(1)	2.376 (9)	Ru(5)–Cl(10)	2.347 (6)
Ru(1)–P(2)	2.35 (1)	Ru(5)–Cl(11)	2.500 (6)
Ru(2)–Ru(3)	3.024 (3)	Ru(5)–Cl(12)	2.297 (7)
Ru(2)–Cl(2)	2.341 (6)	Ru(5)–P(5)	2.347 (7)
Ru(2)–Cl(3)	2.336 (6)	Ru(5)–P(6)	2.361 (7)
Ru(2)–Cl(4)	2.336 (7)	Sb(1)–F(1)	1.84 (2)
Ru(2)–Cl(5)	2.360 (6)	Sb(1)–F(2)	1.77 (2)
Ru(2)–Cl(6)	2.358 (6)	Sb(1)–F(3)	1.84 (2)
Ru(2)–Cl(7)	2.367 (6)	Sb(2)–F(4)	1.82 (3)
Ru(3)–Cl(5)	2.377 (6)	Sb(2)–F(5)	1.90 (2)
Ru(3)–Cl(6)	2.511 (6)	Sb(2)–F(6)	1.76 (3)
Ru(3)–Cl(7)	2.521 (6)	Sb(2)–F(7)	1.60 (4)
Ru(3)–Cl(8)	2.279 (7)	Sb(2)–F(8)	1.74 (4)
Ru(3)–P(3)	2.334 (6)	Sb(2)–F(9)	1.78 (4)
Ru(3)–P(4)	2.344 (7)		

Bond Angles			
Ru(2)–Ru(1)–Cl(1)	129.3 (2)	Cl(7)–Ru(3)–Cl(8)	91.4 (2)
Ru(2)–Ru(1)–Cl(2)	53.2 (2)	Cl(7)–Ru(3)–P(3)	93.8 (2)
Ru(2)–Ru(1)–Cl(3)	52.0 (1)	Cl(7)–Ru(3)–P(4)	169.4 (2)
Ru(2)–Ru(1)–Cl(4)	52.0 (2)	Cl(8)–Ru(3)–P(3)	91.8 (2)
Ru(2)–Ru(1)–P(1)	118.7 (2)	Cl(8)–Ru(3)–P(4)	90.4 (2)
Ru(2)–Ru(1)–P(2)	120.7 (2)	P(3)–Ru(3)–P(4)	96.5 (2)
Cl(1)–Ru(1)–Cl(2)	177.2 (3)	Ru(5)–Ru(4)–Ru(5)	180.00 (0)
Cl(1)–Ru(1)–Cl(3)	94.3 (2)	Ru(5)–Ru(4)–Cl(9)	55.6 (1)
Cl(1)–Ru(1)–Cl(4)	92.2 (2)	Ru(5)–Ru(4)–Cl(9)	124.4 (1)
Cl(1)–Ru(1)–P(1)	91.2 (3)	Ru(5)–Ru(4)–Cl(10)	52.0 (2)
Cl(1)–Ru(1)–P(2)	86.9 (3)	Ru(5)–Ru(4)–Cl(10)	128.0 (2)
Cl(2)–Ru(1)–Cl(3)	88.4 (2)	Ru(5)–Ru(4)–Cl(11)	55.8 (2)
Cl(2)–Ru(1)–Cl(4)	89.0 (2)	Ru(5)–Ru(4)–Cl(11)	124.2 (2)
Cl(2)–Ru(1)–P(1)	88.1 (2)	Cl(9)–Ru(4)–Cl(9)	180.00 (0)
Cl(2)–Ru(1)–P(2)	90.6 (3)	Cl(9)–Ru(4)–Cl(10)	89.6 (2)
Cl(3)–Ru(1)–Cl(4)	82.4 (2)	Cl(9)–Ru(4)–Cl(10)	90.4 (2)
Cl(3)–Ru(1)–P(1)	87.1 (2)	Cl(9)–Ru(4)–Cl(11)	88.9 (2)
Cl(3)–Ru(1)–P(2)	170.5 (3)	Cl(9)–Ru(4)–Cl(11)	91.1 (2)
Cl(4)–Ru(1)–P(1)	169.3 (3)	Cl(10)–Ru(4)–Cl(10)	180.00 (0)
Cl(4)–Ru(1)–P(2)	88.1 (3)	Cl(10)–Ru(4)–Cl(11)	89.4 (2)
P(1)–Ru(1)–P(2)	102.3 (3)	Cl(10)–Ru(4)–Cl(11)	90.6 (2)
Ru(1)–Ru(2)–Ru(3)	174.3 (1)	Cl(11)–Ru(4)–Cl(11)	180.00 (0)
Ru(1)–Ru(2)–Cl(2)	53.4 (2)	Ru(4)–Ru(5)–Cl(9)	51.5 (2)
Ru(1)–Ru(2)–Cl(3)	57.0 (2)	Ru(4)–Ru(5)–Cl(10)	51.8 (1)
Ru(1)–Ru(2)–Cl(4)	56.8 (2)	Ru(4)–Ru(5)–Cl(11)	51.0 (1)
Ru(1)–Ru(2)–Cl(5)	123.9 (2)	Ru(4)–Ru(5)–Cl(12)	126.7 (2)
Ru(1)–Ru(2)–Cl(6)	130.3 (2)	Ru(4)–Ru(5)–P(5)	123.6 (2)
Ru(1)–Ru(2)–Cl(7)	127.3 (2)	Ru(4)–Ru(5)–P(6)	119.3 (2)
Cl(2)–Ru(2)–Cl(3)	92.2 (2)	Cl(9)–Ru(5)–Cl(10)	87.2 (2)
Cl(2)–Ru(2)–Cl(4)	92.7 (2)	Cl(9)–Ru(5)–Cl(11)	82.8 (2)
Cl(2)–Ru(2)–Cl(5)	89.9 (2)	Cl(9)–Ru(5)–Cl(12)	92.6 (2)
Cl(2)–Ru(2)–Cl(6)	176.4 (2)	Cl(9)–Ru(5)–P(5)	173.8 (2)
Cl(2)–Ru(2)–Cl(7)	91.0 (2)	Cl(9)–Ru(5)–P(6)	88.8 (2)
Cl(3)–Ru(2)–Cl(4)	89.0 (2)	Cl(10)–Ru(5)–Cl(11)	85.7 (2)
Cl(3)–Ru(2)–Cl(5)	177.7 (2)	Cl(10)–Ru(5)–Cl(12)	178.0 (2)
Cl(3)–Ru(2)–Cl(6)	90.2 (2)	Cl(10)–Ru(5)–P(5)	91.8 (2)
Cl(3)–Ru(2)–Cl(7)	92.9 (2)	Cl(10)–Ru(5)–P(6)	88.7 (2)
Cl(4)–Ru(2)–Cl(5)	90.0 (2)	Cl(11)–Ru(5)–Cl(12)	92.3 (2)
Cl(4)–Ru(2)–Cl(6)	90.1 (2)	Cl(11)–Ru(5)–P(5)	91.0 (2)
Cl(4)–Ru(2)–Cl(7)	175.7 (2)	Cl(11)–Ru(5)–P(6)	170.0 (2)
Cl(5)–Ru(2)–Cl(6)	87.8 (2)	Cl(12)–Ru(5)–P(5)	88.1 (3)
Cl(5)–Ru(2)–Cl(7)	87.9 (2)	Cl(12)–Ru(5)–P(6)	93.4 (2)
Cl(6)–Ru(2)–Cl(7)	86.1 (2)	P(5)–Ru(5)–P(6)	97.4 (2)
Cl(5)–Ru(3)–Cl(6)	84.0 (2)	Ru(1)–Cl(2)–Ru(2)	73.5 (2)
Cl(5)–Ru(3)–Cl(7)	84.0 (2)	Ru(1)–Cl(2)–Ru(2)	71.0 (2)
Cl(5)–Ru(3)–Cl(8)	175.4 (2)	Ru(1)–Cl(4)–Ru(2)	71.1 (2)
Cl(5)–Ru(3)–P(3)	88.3 (2)	Ru(2)–Cl(5)–Ru(3)	79.3 (2)
Cl(5)–Ru(3)–P(4)	94.2 (2)	Ru(2)–Cl(6)–Ru(3)	76.7 (2)
Cl(6)–Ru(3)–Cl(7)	79.7 (2)	Ru(2)–Cl(7)–Ru(3)	76.4 (2)
Cl(6)–Ru(3)–Cl(8)	95.5 (2)	Ru(4)–Cl(9)–Ru(5)	73.0 (2)
Cl(6)–Ru(3)–P(3)	170.4 (2)	Ru(4)–Cl(10)–Ru(5)	76.2 (2)
Cl(6)–Ru(3)–P(4)	89.7 (2)	Ru(4)–Cl(11)–Ru(5)	73.2 (2)

[a] Numbers in parentheses are estimated standard deviations in the least significant digits.

Table XVI. EPR and Magnetic Susceptibility Data for Linear Trinuclear Ru Complexes with Octahedra Joined on Faces

	μ_{eff}, μ_B/Ru_3	g_1	g_2	g_3
$[Cp_2Co][Ru_3Cl_8(PR_3)_4]$				
R = Bu	1.68	2.23	2.11	1.75
R = Me	1.74			
$Ru_3Cl_8(PR_3)_4$				
R = Bu	0.74		*a*	
R = Et	0.93		*a*	
R = Me			*a*	
$[Ru_3Cl_8(PEt_3)_4][SbF_6]$	1.60	2.43	1.66	

[a] Diamagnetic.

Table XVII. Redox Potentials ($E_{1/2}$ in V) for Linear Trinuclear Ru Complexes with Octahedra Joined on Faces

	oxidn	redn	
	$\sigma_\pi^2\sigma_a/\sigma_\pi^2$	$\sigma_\pi^2\sigma_a^2/\sigma_\pi^2\sigma_a$	
$Ru_3Cl_8(PR_3)_4$			
R = Bu	+0.77	−0.07	−0.92
Ru = Et	+0.81	+0.04	−0.82
R = Me	+0.84	+0.08	−0.80
$[Ru_3Cl_8(PEt_3)_4][SbF_6]$	+0.78	+0.01	−0.90

Table XVIII. ^{31}P NMR Chemical Shifts (ppm) for $Ru_3Cl_8(PR_3)_4$ and Free PR_3

$Ru_3Cl_8(PR_3)_4$	free PR_3	bound PR_3	Δ[a]
R = Me	−62.0	8.30	70.30
R = Bu	−32.72	16.34	49.06
R = Et	−20.11	21.63	41.74

[a] $\Delta = \delta$(bound PR_3) − δ(free PR_3).

that there may be significant ligand to metal charge transfer occurring in this transition. It may explain the relatively large extinction coefficients of the absorption band at 11 900–12 500 cm^{-1}, assuming that the $\sigma \rightarrow \sigma^*$ transition is responsible for the same band.

The results of the Fenske–Hall calculations for the model are in general agreement with those of the SCF–Xα–SW calculations. The energy levels and other pertinent data are listed in Table X. Generally speaking, the energies obtained were more spread out relative to those calculated by using the SCF–Xα–SW method. The ordering of the MOs is likewise and, for the same reason as in the SCF–Xα–SW case, not in total agreement with the ordering predicted by qualitative arguments.

Structural Results. Let us consider first the neutral compounds **3** and **4**. The structures are shown in Figures 11 and 12 and the important bond lengths and angles are listed in Tables XI–XIII. Together with the previously reported PBu_3 compound **1**, we now have four structure determinations of compounds of this type. Key structure parameters for these four, along with corresponding parameters for the $[Ru_3Cl_{12}]^{4-}$ ion are assembled in Table XIV. According to past[3] and present MO calculations, these species all contain Ru–Ru bond orders of $^1/_2$. The structure parameters reflect this. The Cl_b–Ru–Cl_b and Ru–Cl_b–Ru angles show only slight evidence of repulsive force between adjacent Ru atoms, which is consistent with the presence of moderate bonding interactions offsetting what would otherwise be substantial repulsive effects. The Ru–Ru distances vary slightly, from 2.81 Å in $[Ru_3Cl_{12}]^{4-}$ to 2.86 Å in the PEt_3 compound. This range can be said to be characteristic for the complexes of the "Ru_3^{8+}" core.

From the MO results, we see that if one electron is removed, to give a "Ru_3^{9+}" core, it should come from a nonbonding MO, $16b_u$, centered mainly upon the outer Ru atoms. On this basis, no change in Ru–Ru distances would be expected. However, the effect of increasing the formal charge on these atoms from $+2^2/_3$ to +3 will be to increase the electrostatic repulsion and diminish the overlap in the σ-bonding MOs, thus causing a small increase in the Ru–Ru distances. The structure of **5** shows exactly that.

$[Ru_3Cl_8(PEt_3)_4][SbF_6]$ (**5**) crystallized with two crystallographically independent formula units in the unit cell. Each of

the cations, as shown in Figures 13 and 14, has a different disposition of the PEt_3 ligands. In one case the symmetry is C_{2h} (Figure 13), as in the parent $Ru_3Cl_8(PEt_3)_4$ molecule, but in the other the symmetry is lowered to only C_2 (Figure 14). This is reminiscent of the (quite common) occurrence of isomeric forms of the $L_2ClRuCl_3RuClL_2$ molecules.[1] The Ru–Ru distances are slightly different in the two isomers, viz., 2.892 (2) Å for the C_{2h} isomer and 2.914 (3) Å for the C_2 isomer. Other important bond distances and angles are listed in Table XV, and Table XIV gives the average values for the isomeric cations. As expected from the preceeding discussion of the electronic structure, the Ru–Ru distance in the "Ru_3^{9+}" system is a little longer (by ~0.05 Å) than that in the corresponding neutral "Ru_3^{8+}" molecule.

Magnetic and Electrochemical Properties. The magnetic properties of several of the compounds reported here are collected in Table XVI. The three neutral molecules **1**, **3**, and **4** are weakly paramagnetic, which, in view of their closed-shell electronic structures and the absence of EPR signals, we attribute to temperature-independent paramagnetism. Compound **5** shows a larger bulk paramagnetism corresponding to about 1.6 μ_B per trinuclear cation and has an EPR spectrum with two g values of 2.43 and 1.66. The two compounds containing $[Ru_3Cl_8(PR_3)_4]^-$ ions, **8** and **9**, are both paramagnetic with one unpaired electron, and **9** has an EPR spectrum with $g_1 = 2.33$, $g_2 = 2.11$, and $g_3 = 1.75$.

Compounds **1**, **3**, **4**, and **5** all display reversible cyclic voltammograms showing three redox waves. The data are presented in Table XVII. The neutral molecules each have one oxidation wave at +0.80 ± 0.04 V and two reduction waves at 0.00 ± 0.08 and −0.86 ± 0.06 V. Thus, it is to be expected that from these molecules $[Ru_3Cl_8(PR_3)_4]^+$, $[Ru_3Cl_8(PR_3)_4]^-$, and $[Ru_3Cl_8(PR_3)_4]^{2-}$ should be accessible under fairly usual chemical conditions.

For the oxidation to the +1 ion, the use of $AgSbF_6$ has allowed this to be accomplished efficiently in all three cases, thus providing compounds **5**–**7** from **3**, **4**, and **1**, respectively. Compound **5** has three features in its CV that correspond, within experimental uncertainty, to the ones in **3**: these are the same two reduction waves as in **3** and a reduction at +0.78 V corresponding to the oxidation at +0.81 V in **3**.

As for the two reductions to anions, there is good chemical evidence to support these, and there are two compounds containing $[Ru_3Cl_8(PR_3)_4]^-$ ions that have been isolated as their Cp_2Co^+ salts and well characterized, although no crystal structure is yet available. Since the formation of these anions entails the addition of antibonding electrons, it would be predicted that the Ru–Ru distances would increase appreciably over those in the neutral molecules.

^{31}P NMR Spectra. The way in which the chemical shift values vary over the three compounds **1**, **3** and **4** may at first sight appear puzzling, but there is a relationship that is in accord with previous observations. Data are collected in Table XVIII. There is a very good linear relationship between Δ and δ (free PR_3). This type of relationship appears to have first been observed in 1967 for some fluorophosphines in NiL_4 and $M(CO)_3L_3$ compounds,[15] and was again noted in other complexes by Mann et al.,[16] who proposed the relation

$$\Delta = A\delta_{free} + B$$

where A and B are constants characteristic for specific types of complexes. Still other prior cases are known.[17–21]

Concluding Remarks on Preparative Chemistry. The four $Ru_3Cl_8(PR_3)_4$ compounds, **1**–**4**, are best prepared by using stoichiometric quantities of $RuCl_3$ and PR_3 with methanol as reaction solvent. However, the reactions proceed slowly, and only about 40% yields are obtained in 8 days. For **1** and **3** the use of excess phosphine can effect a modest increase in yield (ca. 10%) but when this is attempted for **4** it has the undesirable effect of producing appreciable amounts of $Ru_2Cl_5(PMe_3)_4$ as well. Compound **2** seems always to be accompanied by large amounts of $Ru_2Cl_5(PMe_2Ph)_4$. The electronic spectra of product mixtures are useful in revealing the presence and approximate amounts of contaminants. The tendency toward formation of the dinuclear products seems to be related to the basicity or reducing character of the phosphine, being greater for PMe_3 and PMe_2Ph than for PEt_3 and PBu_3. This is reasonable since the mean oxidation state in the dimers ($+2^1/_2$) is lower than that in the trimers ($+2^2/_3$).

Acknowledgment. We thank the National Science Foundation for support. We also wish to thank Dr. George Bates for the use of the EPR spectrometer.

Supplementary Material Available: Tables of anisotropic displacement parameters and full tables of bond distances and angles (18 pages); listings of calculated and observed structure factors (62 pages). Ordering information is given on any current masthead page.

(15) Reddy, G. S.; Schmutzler, R. *Inorg. Chem.* **1967**, *6*, 823.
(16) Mann, B. E.; Masters, C.; Shaw, B. L.; Slade, R. M.; Stainbank, R. E. *Inorg. Nucl. Chem. Lett.* **1971**, *7*, 881.
(17) Anderson, G. K.; Cross, F. J. *J. Chem. Soc., Dalton Trans.* **1979**, 1246.
(18) Arnold, D. P.; Bennett, M. A. *J. Organomet. Chem.* **1980**, *199*, 119.
(19) (a) Parish, R. V.; Parry, O.; McAuliffe, C. A. *J. Chem. Soc., Dalton Trans.* **1981**, 2098. (b) Al-Sa'ady, A. K. H.; McAuliffe, C. A.; Moss, K.; Parish, R. V. *J. Chem. Soc., Dalton Trans.* **1984**, 491.
(20) Mann, B. E. *Inorg. Nucl. Chem. Lett.* **1971**, *7*, 595.
(21) Mann, B. E.; Muso, A. *J. Chem. Soc. Dalton Trans.* **1980**, 776.